2008-01-01

Comparison of Wave Parameters and Spectra between WERA HF Radars and Tri-Axys Buoys

Mei Wang
University of Miami, mwang@rsmas.miami.edu

UNIVERSITY OF MIAMI

COMPARISON OF WAVE PARAMETERS AND SPECTRA BETWEEN WERA HF RADARS AND TRI-AXYS BUOYS

By

Mei Wang

A THESIS

Submitted to the Faculty
of the University of Miami
in partial fulfillment of the requirements for
the degree of Master of Science

Coral Gables, Florida

December 2008

UNIVERSITY OF MIAMI

A thesis submitted in partial fulfillment of
the requirements for the degree of
Master of Science

COMPARISON OF WAVE PARAMETERS AND SPECTRA BETWEEN WERA HF RADARS AND TRI-AXYS BUOYS

Mei Wang

Approved:

_____ Brian K. Haus, Ph.D. Associate Professor of Applied Marine Physics	_____ Terri A. Scandura, Ph.D. Dean of the Graduate School
_____ Lynn K. Shay, Ph.D. Professor of Meteorology and Physical Oceanography	_____ Hans C. Graber, Ph.D. Professor of Applied Marine Physics
_____ Ad Reniers, Ph.D. Associate Professor of Applied Marine Physics	

WANG, MEI (M.S., Applied Marine Physics)
Comparison of Wave Parameters and Spectra between WERA HF Radars and Tri-Axys Buoys (August 2008)

Abstract of a thesis at the University of Miami.

Thesis supervised by Professor Brian K. Haus.
No. of pages in text. (60)

To establish the credibility of surface wave measurements from two phased-array WERA HF (High Frequency) radars, SEACOOS (SouthEast Atlantic Coastal Ocean Observing System) funded the Mini-Waves experiment from March to May, 2005. For this study, the surface wave parameter (significant wave height) and directional wave spectrum obtained from two WERA radars were compared with those obtained from two Tri-Axys buoys during the same period. The Wyatt (1990) method was used to obtain the directional wave spectra, and significant wave heights were obtained by integrating the directional wave spectra over all directions and the selected frequency band. The SWAN (Simulating WAve Nearshore) directional wave model was used to evaluate the comparison results between WERA radars and buoys. There was a good agreement between WERA radars and Tri-Axys buoys when the echo-Doppler spectrum had a high 2^{nd}-order SNR (signal-to-noise) ratio. The measurements didn't agree in low sea states when the echo-Doppler spectrum had a lower SNR. Also, strong horizontal current shear caused by Florida Current (FC) had an effect on wave propagation direction. To improve the quality of WERA radar wave measurements, a longer sampling interval (10-minute interval) and procedures to remove the effect of RFI are needed.

TABLE OF CONTENTS

Page

LIST OF FIGURES

LIST OF TABLES

Chapter 1 Introduction

1.1 Motivation

Surface waves are an important physical mechanism that influences a number of oceanic processes ranging from CO_2 exchanges between the ocean and the atmosphere to sediment transport and coastline evolution. Routine measurement of ocean surface waves is essential for a variety of marine-related activities, including sea-state forecasts, oceanographic and fisheries research, vessel navigation, and the planning and operation of oceanic engineering projects (offshore structure design). In this context, reliable and effective monitoring of ocean surface waves is of considerate interest and importance.

Reliable ocean surface wave measurements have been an elusive challenge to oceanographers. Available instruments can be categorized into two groups: in-situ and remote sensing. A common and robust in-situ way of measuring surface waves is using a buoy that records the motion of the water surface. The buoy motion provides a time history of the water elevation for that location. Modern wave-rider buoys usually measure their movement along three dimensions, providing information about wave propagation direction. Several wave measurement systems and networks are presently installed in the U.S. The NOAA (National Oceanic and Atmospheric Administration) NDBC (National Data Buoy Center) maintains and operates a network of large wave buoys in order to acquire wave data in deeper ocean basins, coastal waters as well as the Great Lakes.

Buoy measurements are ideal for collecting large quantities of wave data at a specific point. However, buoys are susceptible to theft, vandalism and damage from shipping. Accurate measurements require that the buoy be designed to follow water particles; mooring configuration and buoy hardware can affect measurement performance; deployment and maintenance for long term services are expensive. Moreover, buoys don't work well in regions with strong current such the Gulf Stream.

New remote sensing techniques, ground-, aircraft-, or satellite-based, are capable of measuring the surface wave field locally or globally. For example, SAR (Synthetic Aperture Radar) can potentially measure global directional wave spectra and provide wave pattern information. However, techniques for deriving wave information from SAR images remain complex with limited utilization near coastal area (ports, harbors and bays).

HF (High Frequency)-radars are ground-based remote sensing tools that can be used to measure oceanic parameters. They have the capacity for measuring both directional wave spectra (Wyatt, 1990a; Wyatt and Holden, 1992; Wyatt and Ledgard, 1996) and surface currents over a wide area of the coastal ocean, providing a means of monitoring the simultaneous spatial and temporal variability of surface waves and currents (Shay et al., 2007; Haus et al., 2006; Haus, 2007). To establish the credibility of HF radar wave measurements and, in particular, to assess the accuracy of the measurements, comparisons with existing well-established measuring techniques (such as buoys) are required.

The objectives of this study are to compare significant wave height and directional wave properties from the two WEllen Radar (WERA) HF radars to those

from two Tri-Axys buoys and to establish parameter ranges over which the various platforms are useful for observing directional wave spectra. The aim is to provide a comprehensive thesis on the quality of wave measurements from two ground-based radar systems deployed in Miami at Crandon North Park (CDN) and North Key Largo (NKL). Also, the effects of strong currents and high horizontal current shear on the surface wave observations will be explored.

To improve our understanding of surface wave measurements from HF radars, this thesis is organized as follows. The background with introduction remarks is given in section 1.2. In Chapter 2, the measurements are discussed. Chapter 3 contains the basic theories on HF wave measurements. Comparison results will be given in Chapter 4. Summary and future work will be given in Chapter 5.

1.2 Background

1.2.1 Directional Wave Spectrum

Many offshore applications require information on the directional characteristics of the wave field. These characteristics can be conveniently specified by the directional wave spectrum. The wave energy at a point has an angular distribution as well as a distribution over a range of frequencies. Spectral representations which include both the frequency distribution and the angular spreading of wave energy are known as directional wave spectra.

Mathematically, the surface wave field can be described by the two-dimensional frequency-direction spectrum $S(f,\theta)$, which is often expressed as the product of the omni-directional frequency spectrum $S(f)$ and the directional distribution $D(f,\theta)$, as follows:

$$S(f,\theta) = S(f)D(f,\theta) \quad (1.1)$$

The directional distribution $D(f,\theta)$ has the properties of a probability density function, namely,

$$D(f,\theta) \geq 0 \quad (1.2)$$

where

$$\int_0^{2\pi} D(f,\theta)d\theta = 1 \quad (1.3)$$

The directional spreading function $D(f,\theta)$ is often expressed as a Fourier series

$$D(f,\theta) = \frac{1}{\pi}\left\{\frac{1}{2} + \sum_{n=1}^{\infty}\left[a_n(f)\cos n\theta + b_n(f)\sin n\theta\right]\right\} \quad (1.4)$$

where $a_n(f)$ and $b_n(f)$ are Fourier coefficients.

Measures of the central tendency and variation of $D(f,\theta)$ can be defined in terms of the first ($n=1$) pair or second ($n=2$) pair of Fourier coefficients. In terms of the first pair of Fourier coefficients $a_1(f)$ and $b_1(f)$,

$$\theta_1(f) = \arctan\left(\frac{b_1(f)}{a_1(f)}\right) \quad (1.5)$$

$$\Theta_1(f) = \left\{2\left[1 - \left(a_1^2(f) + b_1^2(f)\right)^{1/2}\right]\right\}^{1/2} \quad (1.6)$$

where $\theta_1(f)$ is defined as the mean wave direction and $\Theta_1(f)$ represents the circular rms (root mean square) spreading.

The analogous definitions in terms of the second pair of Fourier coefficients $a_2(f)$ and $b_2(f)$ are

$$\theta_2(f) = \frac{1}{2}\arctan\left(\frac{b_2(f)}{a_2(f)}\right) \tag{1.7}$$

$$\Theta_2(f) = \left\{\frac{1}{2}\left[1 + \left(a_2^2(f) + b_2^2(f)\right)^{1/2}\right]\right\}^{1/2} \tag{1.8}$$

where $\theta_2(f)$ is defined as the dominant wave direction and $\Theta_2(f)$ the directional spreading factor.

Two main classes of gravity waves exist in the ocean, namely, the so-called wind-wave and swell. The former refers to young (or developing) waves under growth or ultimately in equilibrium with local wind, while the latter is defined as waves generated elsewhere and propagating over large distances. Wave age, defined as $C_p/U_{10} << 1.2$, where C_p is the phase velocity of the gravity wave and U_{10} the wind speed at a height of 10 m above the sea surface, can be taken as a criteria to separate wind-wave from swell (Donelan, 1990). In practice, many coastal and offshore engineering applications require detailed knowledge of wave conditions at specific locations. Such information is not usually available due to incomplete and discontinuous wave observations in coastal regions.

In such cases, predictions of the wave conditions by numerical models become a popular tool, since they may provide the good estimates of wave information at specific locations for given wind fields. An example of such a model is the SWAN (Simulating WAve Nearshore) model, a 3rd-generation wave model used to compute directional spectra of random short-crested waves in coastal waters. SWAN has been

developed by Booij et al. (1999) and evaluated especially in coastal regions with shallow waters, islands (barriers), tidal flats, local wind, and ambient currents. In SWAN, the evolution of wave spectrum is described by the action balance equation, since the wave action density spectrum is conserved in the presence of currents. The spectral action balance equation in cartesian coordinates that SWAN uses to describe the evolution of the wave spectrum is (Hasselmann et al., 1973):

$$\frac{\partial}{\partial t}N + \frac{\partial}{\partial x}c_x N + \frac{\partial}{\partial y}c_y N + \frac{\partial}{\partial \omega}c_\omega N + \frac{\partial}{\partial \theta}c_\theta N = \frac{S_{source}}{\omega} \tag{1.9}$$

where $N = N(\omega,\theta)$ is the action density spectrum related to the energy density spectrum $S(\omega,\theta)$ by $N(\omega,\theta) = S(\omega,\theta)/\omega$; ω is the relative frequency as observed in a frame of reference moving with the action propagation velocity and θ is the wave propagation direction defined as the direction normal to the wave crest of each spectral component; the first term at the left-hand side of Eq. (1.9) accounts for the local rate of change of action density in time; second and third terms represent the propagation of action in geographical space; the fourth term represents shifting of the relative frequency due to variations in depths and currents; the fifth term represents refraction; on the right-hand side S_{source} is the source term in terms of energy density representing the effects of generation, dissipation and non-linear wave-wave interactions.

1.2.2 HF Radar Wave Measurement

Ocean remote sensing using HF radar is based on the measurement of backscattered power from moving ocean surface. The HF band encompasses frequencies between 3 and 30 MHz with corresponding electromagnetic wavelengths between 100 and 10 m. HF remote sensing is based on sky-wave or ground-wave propagation. Sky-wave propagation makes use of the refraction by the ionosphere to achieve large-scale ranges. However, the ionosphere undergoes temporal changes and modulates the signal from the sea surface (Gurgel et al., 1997). For the ground-wave propagation, the radio wave is transmitted from the shore with vertical polarization so that it propagates along the air-sea interface. This is a high-loss mode of propagation and the radar range is 10-100 times less than the range for sky-wave propagation. However, the advantages of the ground-wave mode are that the spectra are uniquely derived from the ocean backscatter and the grid is more accurately determined for mapping the derived physical parameters. Here we focus on the ground-wave propagation only. Parts of the transmitted HF power (ground-wave) propagate along the sea surface following the Earth's curvature beyond the horizon. When the pulse is scattered back from the ocean surface, the RCS (Radar Cross Section) corresponding to the sampled patch is known and it is proportional to the sea-state. Moreover, since the transmitted pulse scatters from the moving ocean surface, a Doppler shift in the transmitted frequency is induced at the receiving antenna. Figure 1.1 shows a typical measurement from a radar system working in the HF range and looking at near-grazing incidence angle. Such a diagram is known as backscattered Doppler spectrum and it represents the power backscattered from the

surface waves moving within the ocean patch sampled. The backscattered power spectrum is obtained by the Fourier transformation of the in-phase (*I*) and quadrature (*Q*) time series of the scattering surface waves. The spectral resolution and noise suppression depend on the deviation of sampling.

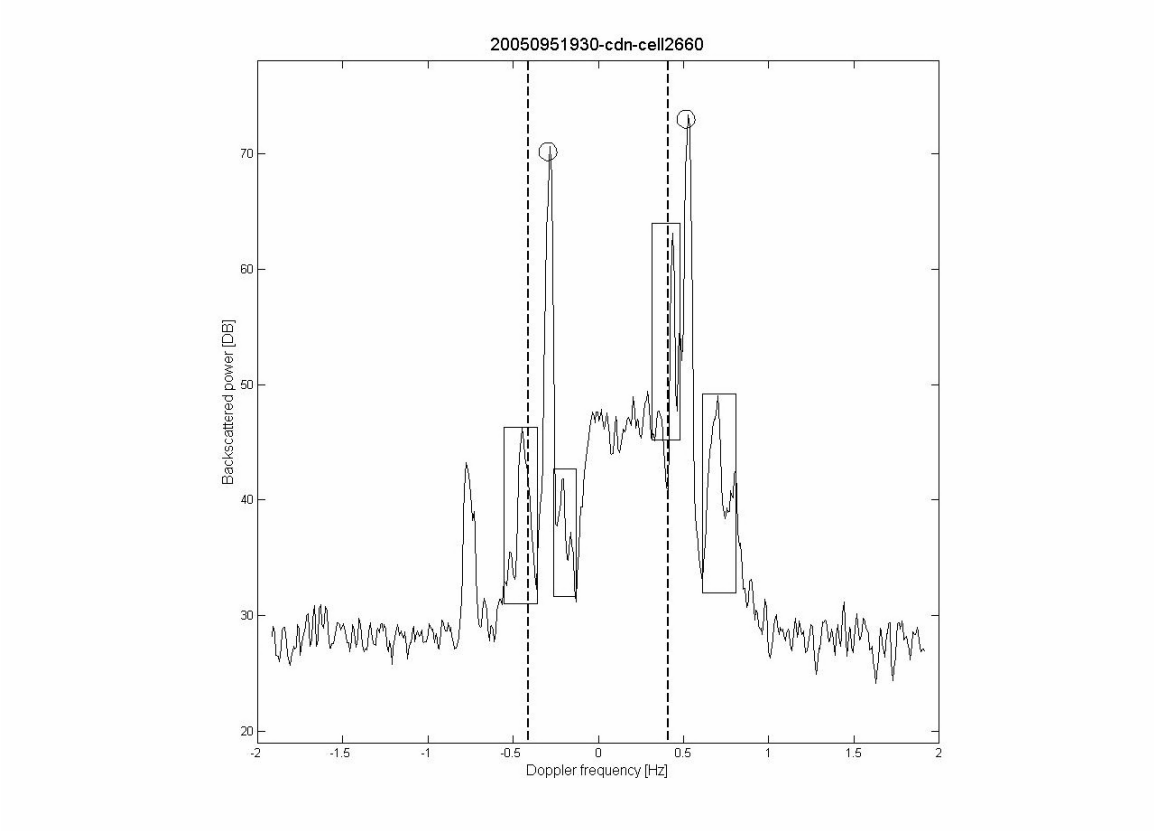

Figure 1.1. Backscattered Doppler spectrum recorded at 1930 UTC 5 April 2005. The measurement was made by a shore-based radar system on CDN (Crandon North park) working in HF mode (16.045 MHz). Two 1st-order Doppler peaks are shown with circles. Four 2nd-order sidebands are shown with rectangular areas. Bragg frequencies are shown as dashed lines corresponding to 0.41 Hz for a 16.045 MHz transmission frequency.

The basic physics on HF remote sensing was the subject of research for many years since World War II, but the first major contribution to this field was introduced by Crombie (1955) who described the presence of the two prominent peaks in the Doppler spectrum (1st-order peaks in Figure 1.1). Crombie found that

the resonance conditions between the electromagnetic pulse emitted by the radar and a single ocean wave with a particular wavelength (half of the radar wavelength) were responsible for the abrupt increase in backscattered power at two particular frequencies known as Bragg frequencies (± 0.41 Hz in Figure 1.1). He also found that the difference between the Doppler frequencies corresponding to these peaks and their theoretical values was caused by the underlying current field which caused advection of the entire wave field. This notion led to the development of radar systems to be used to measure ocean surface currents.

Hasselmann (1971) proposed the concept of 2nd-order hydrodynamic and electromagnetic interaction giving rise to continuous 2nd-order sidebands in addition to two discrete 1st-order Doppler lines. He suggested that the 2nd-order sidebands around each 1st-order peak are proportional to the frequency-wave height spectrum. Thus, the integral of normalized sidebands should determine the significant wave height. Barrick (1972) derived a transfer function which related the 2nd-order radar cross section to the two-dimensional wave height spectrum of ocean surface waves. The theory is based on a perturbation expansion and the assumption that the sea surface is a perfect conductor. In principle, Barrick's theory (1972) allows the estimation of the two-dimensional wave height spectrum by inverting a nonlinear integral equation. This problem has been studied by a number of authors, e.g. Wyatt (1990; 1999), Howell and Walsh (1993) and Hisaki (1996). By comparison with buoy data, Wyatt et al. (1999) have found that the inversion procedure produces a useful accuracy on the inversion of wave spectra. The authors conclude that this radar remote sensing approach has a potential for operational coastal monitoring and sea-state forecasting.

1.2.3 Wave-Current Interaction

When ocean waves propagate through a region with a varying current, wave propagation direction, wavelength, and wave heights are altered by wave refraction. Wave-current interaction is a complicated subject to deal with mathematically. This is not surprising; physically this is a problem of wave propagation in an inhomogeneous, non-isotropic, dispersive, dissipative, and moving medium, which also interacts with the wave. Furthermore, the current velocity will vary over depth due to bed friction, wind stress and stratification. Wave-current interaction was studied by Longuet-Higgins and Stewart (1960, 1961). They presented the correct energy equation for a wave superimposed on a variable current, thus introducing the important concept of radiation stress. Subsequently, a different energy approach was introduced for waves on large-scale currents: wave action conservation between so-called rays (Bretherton and Garrett, 1968).

When ocean waves propagate over uniform currents, there are two primary effects on wave propagation, which have been divided into effects on wave kinematics and dynamics (Jonsson, 1990). The kinematic effects for ocean waves include effects on the wave phase velocity and the wavenumber. The absolute phase velocity for waves moving over uniform currents will be shifted away from the relative phase velocity by the current component in the wave direction. Also, the wavelength will be proportionally shortened (lengthened) in an opposing (following) current. The dynamic effects on the surface waves over uniform currents can be derived from energy or action conservation equations (Mei, 1984). Wave heights will increase (decrease) when waves are moving against an opposing (following)

current. The strength of this effect depends on the incident wavenumber and propagation direction relative to the current direction.

For horizontally sheared currents, the wave propagation direction will also change since the wave propagation speed changes as waves move across variable currents or topography. For waves propagating obliquely into a sheared current their ray-paths will be curved. Kenyon (1971) demonstrated that in cases of weakly sheared flow and weak current magnitude (U^0) relative to the wave group velocity (C_g), such that $U^0/C_g << 1$ the ray curvature (ψ) is approximately equal to the ratio between C_g and the surface current vorticity (υ)

$$\psi = C_g / \upsilon \tag{1.10}$$

where $\upsilon = \left(\frac{\partial U_y^0}{\partial x} - \frac{\partial U_x^0}{\partial y} \right)$. This result has several important implications. First, for a given current field the radius of curvature increases in proportion to the group velocity. Furthermore following (opposing) waves traveling over a sheared current will be refracted in the direction of decreasing (increasing) current field. MacIver et al. (2006) measured wave refraction on both horizontally and vertically sheared currents in the laboratory. Their results confirmed the basic structure predicted by ray theory based on the mild shear assumption. They observed opposing waves bending toward the current normal and increasing in height and following waves bending toward current parallel and decreasing in height.

Nadai (2006) has analyzed the influence of wave-current interaction on the current measurement of HF radar by means of a simulation of the 1st-order Doppler echo spectra and the radar sensitivity distribution. Due to the conservation of the

wave action, the local spectral density of ocean waves strengthens where the ocean waves propagate against the current, while it weakens where the ocean waves propagate following the current. The local spectral density is also affected by the divergence of the current field. The local spectral density determines the NRCS (Normalized Radar Cross Section) of the 1st-order echo. Therefore, the NRCS has a non-uniform distribution as a result of wave-current interaction. Nadai (2006) has pointed out that there will be a significant effect on current observations from HF radar in regions of strong surface current shear. However, the effect of wave-current interaction on the wave observations from HF radar is unknown. This thesis will give some preliminary results on this area.

Chapter 2 Datasets

This chapter presents a description of the data acquired to evaluate the performance for directional wave spectra measurement of overlapping phased-array radar systems. This chapter will be organized as follows. An experiment to study HF radar observations in strong currents will be discussed in section 2.1. The other datasets used in this thesis will be discussed in section 2.2.

2.1 Mini-Waves Experiment

Phased-array HF radar offers promise in not only resolving the surface current field, but also in observing the spatial variability of significant wave heights and directional properties of the waves. Briefly, significant wave heights are proportional to the 2^{nd}-order returns in the Doppler spectrum normalized by the 1^{st}-order returns (Barrick, 1977). Directional wave properties may also be obtained through the inversion of a nonlinear integral equation using the 2^{nd}-order returns (Wyatt, 1990). There are several methods using HF radar data from phased arrays. All the studies stress the importance of having concurrent in-situ measurements to calibrate and validate these empirical approaches.

For this purpose SEACOOS (SouthEast Atlantic Coastal Ocean Observing System) funded a field experiment (Mini-Waves) with multi-institution participation where two Tri-Axys directional buoys and several RD Instrument ADCPs (Acoustic Doppler Current Profiler), Sontek ADPs (Acoustic Doppler Profiler) and one Nortex current meter were deployed within the coverage region of two WERA (WEllen

RAdar) stations offshore of SE (SouthEast) Florida from March to May, 2005 (Voulgaris et al., 2008). These in-situ data are used to calibrate radar returns and determine empirical coefficients for computation of wave parameters.

2.1.1 Experiment Venue (Florida Straits)

The Straits of Florida is located south-southeast of the North American mainland, generally accepted to be between southeast Florida and Bahamas and Cuba. The Florida Strait carries the Florida Current, the beginning of the Gulf Stream, starting from the Gulf of Mexico. The Florida Straits is an almost ideal area in which to study the effects of strong currents and current shear on wave propagation, due to the presence of the Florida Current. The region is also rarely exposed to non-locally generated swell waves which are dissipated over the shallow banks of the islands of the Bahamas lying about 100 km to the east. Typical current velocities within the FC exceed 1.5 m s^{-1} and at times have exceeded 2.2 m s^{-1}. There are high lateral shear zones along both edges of the FC; however, the strongest shears typically are observed along the western boundary (http://en.wikipedia.org/wiki/Florida_Current).

2.1.2 Instruments

2.1.2.1 WERA HF Radars

The first commercial application of HF radar was the CODAR (Coastal Ocean Dynamics Applications Radar) system, introduced in 1977 by D. E. Barrick at

NOAA. This system has initially been designed for mapping surface current fields only. In 1996, an HF radar called WERA (WEllen RAdar) was developed at the University of Hamburg (Gurgel, 1999) to be a more flexible tool for research. WERA can be used for mapping surface current fields (Shay et al., 2007; 2008) and surface wave fields (Haus, 2007).

The HF radars used for Mini-waves experiment are two WERA radars located along the SE Florida coast since June 2004. Since then the two WERA radars have collected Doppler spectra quasi-continuously every 20 minutes. Both of these WERA radars consist of transmit/receive stations with a rectangular 4-element transmitter and a linear 16-element phased-array receiver (Table 2.1). The operating frequency for these two WERA HF radars is 16.045 MHz, the corresponding Bragg wavelength is 9.35 m and the range cell resolution is 1.2 km. The two WERA radars transmit FMCW (Frequency Modulated Continuous Wave) signals to investigate ocean surface processes. The two radar stations were positioned at a distance of ~ 50 km from each other (Figure 2.1). This provides a large coverage area for current measurements, with the region of consistent current vector retrievals extending well out over the Florida Straits. The retrieval method, Wyatt's (1990) approach for surface wave measurement requires that the observations from two overlapping radar stations be available as in the case for current vectors. However, because 2^{nd}-order returns have lower Signal-to-Noise Ratio (SNR) than the 1^{st}-order returns their use is usually limited to about 50% of the range over which current measurements are obtained. At the operating frequency of 16.045 MHz, the range for current measurements is about 80-100 km and the range for wave measurements is about 40-50 km. This makes the overlapping requirement much more restrictive for wave

observations than for current observations (Wyatt et al., 2005). Moreover, the large distance between stations limited the region for which directional wave spectra could be measured using dual-site methods to a relatively small area (Wyatt et al., 2005).

Echo-Doppler spectra have been archived at each radar station since June 2004. During the period of Mini-Waves (March-May, 2005), two WERAs actively transmitted and received signals for 5 minutes (1024 samples) successively from each site, with the measurement cycle repeated every 20 minutes.

Operating Frequency	16.045 MHz
Transmitted Peak Power	30 Watts
Bragg Wavelength	9.35 m
Measurement Depth	~ 0.8 m
Operational Range for Currents	80-100 km
Operational Range for Waves	40-50 km
Range Cell Resolution	1.2 km
Integration Time	5 minutes
Azimuthal Resolution (3 Db down)	2^{o}
Radial Doppler Velocity Resolution	2 cm s^{-1}

Table 2.1. WERA system characteristics as deployed over the SouthEast Florida Shelf during the mini-waves experiment.

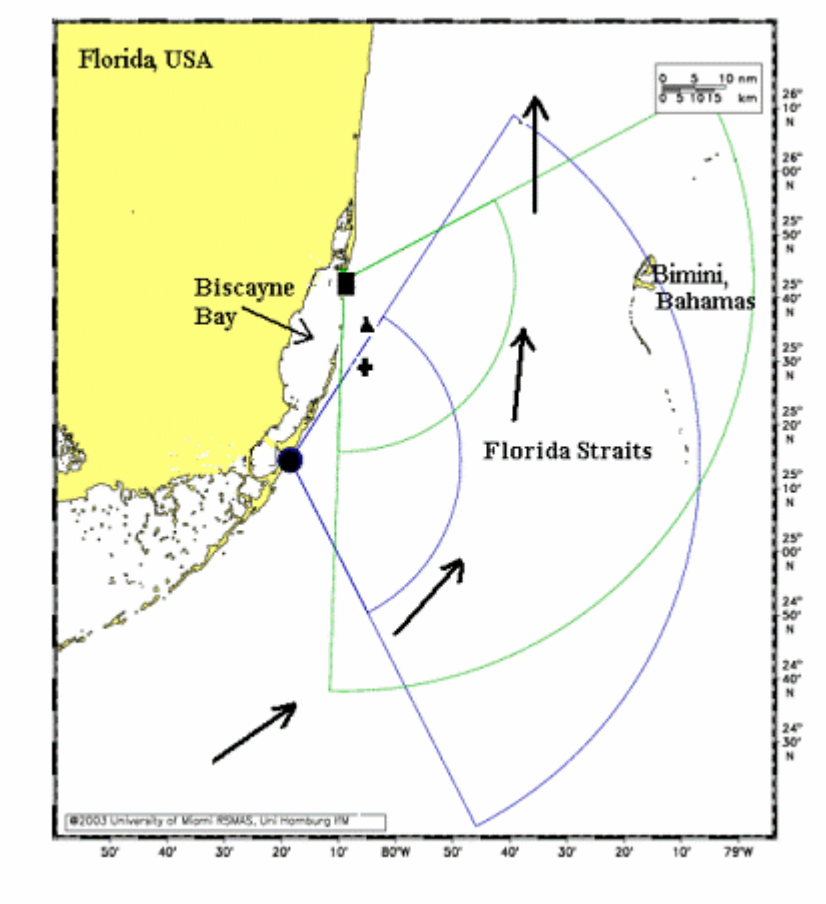

Figure 2.1. Coverage area of WERA stations as deployed for SEACOOS. Outer semicircle is the radial coverage from each station. Inner semicircle is the typical wave measurement limit from each station. Solid black square (■) denotes the location of the Crandon North Park (CDN) WERA site. Solid black circle (●) is the North Key Largo (NKL) WERA site. Triangle (▲) denotes the location of FWYF1 used for wind and air-sea temperature measurements. Cross (+) marks the location of 8 in-situ instruments used for wave measurement calibration and validation. Black thick arrows show the general flow direction of the Florida Current (FC). (Haus, 2007)

2.1.2.2 In-situ Instruments

There was a combination of in-situ sensors deployed along the shelf break within the radar domain (Figure 2.1) from YD (YearDay) 75 to YD 145. These in-situ sensors consist of several upward-looking, bottom-mounted mode RD

Instrument ADCPs Sontek ADPs, one Nortek current meter and two Tri-Axys buoys. Figure 2.2 provides the expanded view of in-situ instrument locations. Hourly wave observations were recorded by these in-situ sensors based on 20-minute burst sampling at the beginning of each hour. Since wave measurements by Tri-Axys buoys are used here to evaluate HF radar wave measurements in this thesis, we will focus on the wave measurements obtained from the two Tri-Axys buoys only.

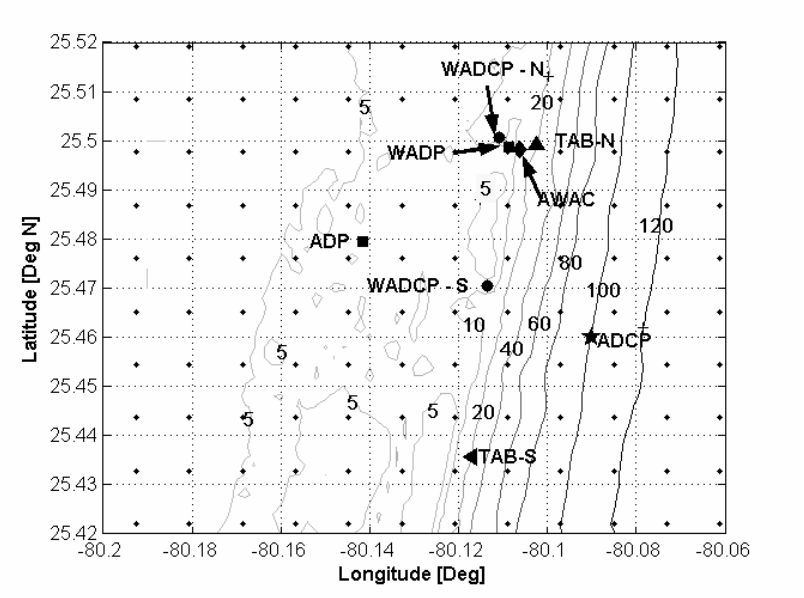

Figure 2.2. Expanded view of in-situ instrument locations during Mini-Waves Cal-Val experiment. WADP-1500 KHz Sontek ADP with wave package, WADCP-1200 KHz RDI waves ADCP. AWAC-Nortek current meter. TAB-N,S-Tri-Axys directional wave buoys. Depth contours shown with depths in meters. (Haus, 2007)

The Tri-Axys directional wave buoy is the result of a collaborative development and testing program between Axys Technologies Inc. and the Canadian Hydraulics Centre (CHC) of the National Research Council of Canada (Figure. 2.3). The Tri-Axys buoy is a water particle-following buoy that measures the buoy accelerations motion in three orthogonal directions. The buoy uses three accelerometers to

measure total accelerations along the mutually orthogonal X, Y, Z axes of the buoy; three angular rate sensors measure rotation rates about the roll, pitch and yaw axes and a gimbaled compass measures sensor heading. Since the full non-linear equations of motion are used, accurate motion data are obtained for extreme conditions with roll and pitch angles up to 60 degrees.

During Mini-Waves, each Tri-Axys buoy recorded time series describing the output from three accelerometers and three gyros that define angular motion (Voulgaris et al., 2008). These sensors were sampled at 4 Hz for the first 20 minutes of each hour. The resulting time series were used to compute heave and horizontal velocities of the buoy, and these time series were processed within the buoy to compute directional energy spectra. The buoy is assumed to follow the water surface and thus report its motions. The buoy utilizes the Maximum Enthalpy Method (MEM) to obtain the directional wave spectra. An upper limit of 0.64 Hz is imposed on the computed non-directional wave energy spectra, with energy above this limit assumed to be due to noise. Similarly, energy appearing below 0.03 Hz is neglected and assumed to be a byproduct of noise in the accelerometers.

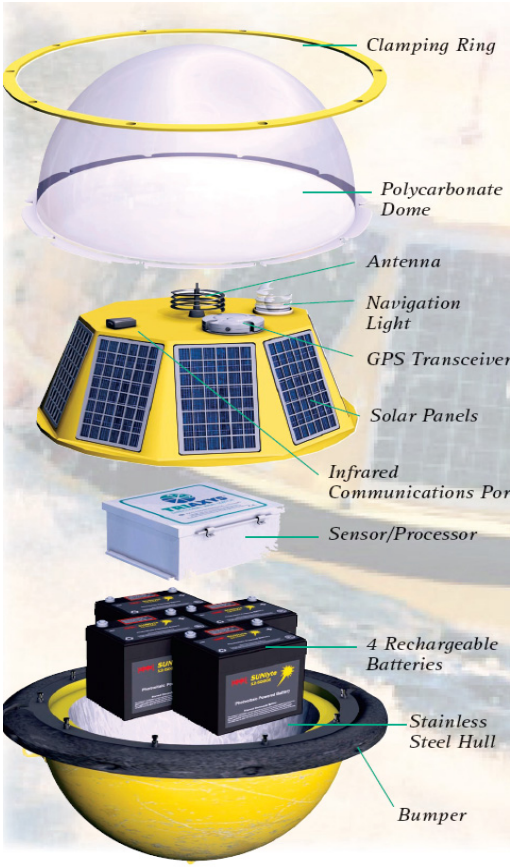

Figure 2.3. Major components of Tri-Axys directional wave buoy.

Both of the two Tri-Axys buoys report directional wave energy spectra, from which non-directional spectra and bulk parameters defining wave height, period and propagation direction. The significant wave is defined as

$$H_s = 4.01\sqrt{m_0}\,, \tag{2.1}$$

where $m_0 = \int_{f_{low}}^{f_{high}} E(f)df$ is the total integrated energy within the wave spectrum, between the lower and upper cut-off frequency.

2.2 Other Datasets

For this study, a NOAA CMAN station was used to obtain the wind information and meteorological information, and SWAN model results were used for the inter-comparison of the directional wave spectra.

2.2.1 FWFY1 Wind and Meteorological Data

Wind speed and direction and air and sea-water temperatures were available at the NOAA CMAN (FWFY1) station, maintained by NDBC (Figure 2.1). FWFY1 is located at Fowey Rocks, FL (Figure 2.1). The station is on a tower mounted in ~ 3 m of water along the outer edge of the reef tract. The anemometer at FWFY1 was 43.9 m above the mean water level (MWL). The air temperature was recorded 11 m above MWL and the water temperature was recorded 1 m below MWL. A neutrally stable log-profile was used to convert the observed wind speed to an equivalent neutral 10-m wind speed. A six-day time series in April 2005 was selected for this study (YD 95 - YD 100) (Figure 2.4). Inspection of the wind record revealed one period (YD 95 – YD 98) when the onshore wind direction was relatively steady with a wind speed ranging from 4 to 14 m s^{-1} (Figure 2.4).

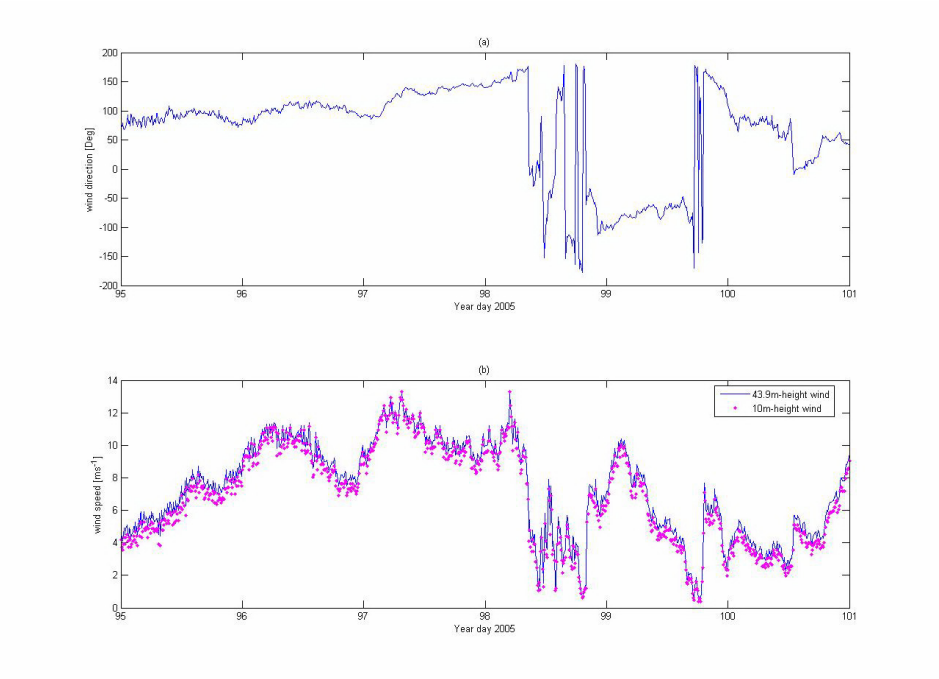

Figure 2.4. FWFY1 CMAN station observed winds at height of 43.9 m during April 2005 converted to 10-m neutral values. (a) Wind direction (from) in degrees clockwise from true North. (b) Wind speed (m s^{-1}).

2.2.2 SWAN Wave Model Results

SWAN (Simulating WAve Nearshore, http://swan.ct.tudeflt.nl/) is a numerical wave model for obtaining realistic estimates of wave parameters in coastal areas. SWAN is based on the discrete spectral action balance equations. The action balance equation is solved with a full discrete 2- dimensional wave spectrum and an iterative technique is applied to allow propagation of waves in all directions over the domain. For this study, SWAN was configured to the Florida Straits, and the domain for Mini-Waves was encompassed by the SWAN model operation domain (Figure 2.5). SWAN was operated on the same domain obtained from the current map image from the two WERA HF radars on 1300 GMT, April 5th, 2005. SWAN used hourly-

averaged wind field obtained from FWFY1 tower as the initial wind forcing which was assumed to be uniform over the SWAN domain. Using the observed current field obtained from two WERA HF radars and winds from FWFY1 tower, SWAN provided the simulated directional wave spectra on each grid. Note that the spatial resolution for SWAN is 4.86 km in latitude and 3.66 km in longitude, the frequency resolution is 0.01 Hz and the azimuthal resolution is 10 degrees.

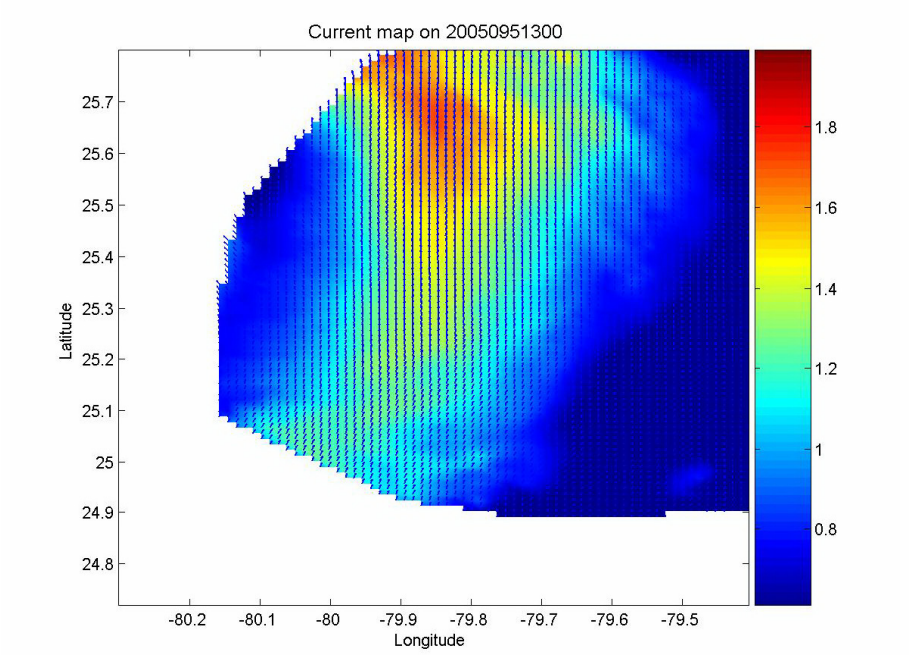

Figure 2.5. Current map obtained by WERA on 1300 GMT, April 5th, 2005. Color contours denote the current magnitudes and the arrows denote the current directions.

Chapter 3 Methods

This chapter is focused on the methods used to retrieve significant wave height and directional wave spectra from 2nd-order returns from the Doppler spectrum. Section 3.1 will review the basic theories of HF radar wave measurements. Section 3.2 will focus on Wyatt (1990) relaxation method.

3.1 Reviews of Basic Theories of HF Radar Wave Measurement

A typical echo-Doppler spectrum is characterized by two dominant peaks positioned roughly symmetrically around zero Doppler. These discrete 1st-order Bragg peaks are caused by ocean waves (known as Bragg waves) of half of the radar wavelength traveling towards or away from the radar site (Figure 1.1).

$$\mathbf{k_B} = \pm 2\mathbf{k_r}, k_r = \omega_r / c, \tag{3.1}$$

where the wave-number k_r is the modulus of the horizontal HF wave vector $\mathbf{k_r}$, ω_r the HF transmitted circular frequency, and c the speed of light ($2.998 \times 10^8\ ms^{-1}$).

The moving Bragg waves induce a Doppler shift to the backscattered HF signal,

$$\omega_d = \pm \omega_B - 2\mathbf{k_r} \cdot \mathbf{u}, \tag{3.2}$$

where ω_B is related to the wave-number k_B by the deep-water dispersion relation,

$$\omega_B = \pm \sqrt{g k_B}, \tag{3.3}$$

where g is the gravitational acceleration ($9.81 ms^{-2}$). The sign in front of ω_B depends on the direction of the scattering Bragg wave relative to the radar. The first

term in Eq. (3.2) is due to the phase velocity of the Bragg waves and the second term due to the underlying current. The capability of an HF radar of measuring the radial current component of surface current velocity is based on Eq. (3.2).

An underlying surface current with radial component u towards the radar causes a Doppler shift of Δf Hz in the Doppler spectrum,

$$\Delta f = 2u/\lambda_r \,, \tag{3.4}$$

or

$$\Delta\omega = 2\mathbf{u}\cdot\mathbf{k_r}\,, \tag{3.5}$$

where λ_r is the radar wavelength.

Identification of this frequency shift yields an estimate of the radial component of surface current. Radial measurements from multiple radar sites can be combined together to resolve two-dimensional (2-D) current vectors.

In addition to the 1st-order returns, there are four continuous 2nd-order sidebands surrounding the two Bragg peaks. The 2nd-order returns contain backscattered energy resulting from multiple reflections of the radar signal as well as the hydrodynamic combination of surface waves to produce Bragg scattering (Barrick, 1977b). Therefore, the 2nd-order returns contain information on the surface waves.

The first comprehensive theory of radar pulse scattering from the ocean surface (Scattering theory) was introduced by Barrick in the early 70's (Barrick, 1972a, 1972b). Based on the theory of vertically polarized electromagnetic signals approaching at near-grazing incidence angles and scattering from random rough sea surfaces, Barrick derived expressions to estimate the prominent 1st-order Bragg peaks and the background 2nd-order sidebands of the Doppler spectrum.

To 1st-order, the Doppler spectrum can be expressed in terms of the average radar cross section per unit (mean) sea surface area per rad s^{-1} bandwidth as

$$\sigma_{(1)}(\omega_d) = 2^6 \pi k_r^4 \sum_{m'=\pm 1} S(-2m'\mathbf{k_r})\delta(\omega_d - m'\omega_B), \tag{3.6}$$

where ω_d is the radian Doppler frequency of the received signal, m' denotes the sign of the Doppler shift, $\mathbf{k_r}$ is the radar wave vector of magnitude k_r and direction towards the scattering patch from the radar, $S(\mathbf{k})$ is the ocean directional wave-number spectrum, $\omega_B = \sqrt{2gk_r \tanh(2k_r d)}$ is the Bragg frequency, d is the water depth and δ is the Dirac-delta function. This equation describes two peaks located at $\pm\omega_B$ with amplitudes dependent on the amplitudes in the directional spectrum along the radar beam direction towards, $S(-2\mathbf{k_r})$, and away, $S(+2\mathbf{k_r})$, from the radar. In general, the product $S(-2m'\mathbf{k_r})\delta(\omega_d - m'\omega_B)$ represents a mapping of the wave energy spectral ordinates from the wave-number domain to the frequency domain according to the definition of the dispersion relation. However, the product represents a mapping of the wave energy spectral ordinates from the wave-number domain to the Doppler frequency domain and it is non-zero for $\omega_d = \pm\omega_B$ only. Theoretically, the backscatter power to the 1st-order is limited to a single peak at the positive and negative Bragg frequencies in the Doppler spectrum. This feature is clearly apparent in Figure 1.1, where the 1st-order peaks reach values between 40 and 45 dB above the noise floor level.

The 2nd-order contribution to the radar cross section is given by:

$$\sigma_{(2)}(\omega_d) = 2^6 \pi k_r^4 \sum_{m,m'=\pm 1} \int_{-\infty}^{+\infty}\int_{-\infty}^{+\infty} |\Gamma_T|^2 S(m\mathbf{k}) S(m'\mathbf{k}') \times \delta(\omega_d - m\sqrt{gk\tanh kd} - m'\sqrt{gk'\tanh k'd})\,dpdq \tag{3.7}$$

where the integration variables p and q are wave-number components parallel and perpendicular to $\mathbf{k_r}$, respectively, and are related to the three wave vectors, $\mathbf{k}$, $\mathbf{k}'$ and $\mathbf{k_r}$ by $\mathbf{k} = (p - k_r, q)$ and $\mathbf{k}' = (-p - k_r, -q)$ so that $\mathbf{k} + \mathbf{k}' = -2\mathbf{k_r}$. Here m and m' (both equal to ± 1) locate the 2nd-order contribution either to the left or the right of the 1st-order peaks. Γ_T is the coupling coefficient describing both the electromagnetic and hydrodynamic processes that provide the 2nd-order backscatter.

Hasselmann (1971) initially suggested that the 2nd-order Doppler sidebands around each 1st-order peak are proportional to the wave-height non-directional temporal spectrum, centered at the 1st-order Bragg frequency, $\pm\omega_B$. If this were strictly true, the area under these sidebands would be proportional to the mean-square sea wave height.

The ocean wave directional spectrum is related to the 2nd-order continuous sidebands of the Doppler spectrum by means of a nonlinear integral equation (Barrick, 1977). The extraction of ocean wave directional spectrum is not a straight-forward task and many different approaches have been proposed (Howell and Walsh, 1993; Wyatt, 1990; Hisaki, 1996; Hashimoto and Tokuda, 1999). There are two classes of methods for this inversion problem: linear and non-linear. Howell and Walsh (1993) and Wyatt (1990) method are linear ones, while the Hisaki (1996) method is a non-linear one. Howell and Walsh (1993) present a numerical inversion method to calculate a direct solution to the HF-radar integral equation for the case of

one or more radars with a narrow-beam antenna system deployed in a mono-static configuration (transmitter and receiver in the same location). First of all, they normalize the radar Doppler spectrum by the energy contained in the 1st-order peaks; then, they approximate the integral equation as a matrix equation via a Fourier decomposition; finally, a direct solution to the matrix equation is found by using a singular value decomposition. Their method is suitable for near real-time analysis of HF radar data. Wyatt (1990) has developed an iterative inversion method to estimate the directional spectrum. For this thesis, the Wyatt (1990) method is used to invert the integral equation derived by Barrick to obtain the directional wave spectrum (Section 3.2). Hisaki (1996) presents a method to solve the nonlinear integral equation without linearization or approximation. He modifies the nonlinear integral equation to a discretized form and adds the constraints to obtain a stable solution. Hisaki converts the nonlinear integral equation into an optimization problem and proposes a simple algorithm to solve this problem.

3.2 Wyatt (1990) Method

Wyatt (1990) started from the Barrick's equations for the 1st- and 2nd-order radar cross section (Eq. (3.6) and Eq. (3.7)). Normalized by the Doppler frequency ω_d and wave-number by ω_B and $2k_r$, respectively, Barrick's equations can be written in dimensionless form as

$$\sigma_{(1)}(\eta,\phi,D) = 4\pi \sum_{m'=\pm 1} S(1,(1+m')\pi/2)\delta(\eta - m') \tag{3.8}$$

$$\sigma_{(2)}(\eta,\phi,D) = 8\pi \sum_{m,m'=\pm 1} \int_0^{+\infty} \int_{-\pi}^{\pi} |\gamma_r|^2 S(K,\alpha) S(K',\alpha') \times \delta(\eta - m\sqrt{K \tanh KD} - m'\sqrt{K' \tanh K'D}) K dK d\theta \tag{3.9}$$

$$\alpha = \theta \pm (1-m)\pi/2 \tag{3.10}$$

$$\alpha' = \theta \pm (1-m')\pi/2 \tag{3.11}$$

where $\eta (= \omega_d / \omega_B)$ is the normalized Doppler shift, $D = 2k_r d$ is the normalized water depth, and ϕ is the radar bearing. γ_t is the dimensionless coupling coefficient ($\gamma_t = \Gamma_T / 2k_r$) describing both the electromagnetic and hydrodynamic processes that provide the 2nd-order backscatter. K and K' are normalized wave-numbers, $K = k / 2k_r$ and $K' = k' / 2k_r$, respectively. θ is the radar look-direction measured counter-clockwise from the east direction. m and m' define the four 2nd-order sidebands of the Doppler-spectrum: 1) $m = m' = 1$ corresponds to $\eta > 1$; 2) $m = -1, m' = 1$ corresponds to $0 < \eta < 1$; 3) $m = 1, m' = -1$ corresponds to $-1 < \eta < 0$; and 4) $m = m' = -1$ corresponds to $\eta < -1$. Applying the properties of the Dirac delta function to evaluate one of the integrals in closed form, the 2nd-order equation (3.9) then becomes

$$\sigma_{(2)}(\eta,\phi,D) = 16\pi \sum_{m,m'=\pm 1} \int_{-\pi}^{\pi} |\gamma_t|^2 J_t S(K,\alpha) S(K',\alpha') K^{\frac{3}{2}} d\theta \tag{3.12}$$

where J_t is the Jacobian required for the transformation and the restrictions

$$\eta - m\sqrt{K \tanh KD} - m'\sqrt{K' \tanh K'D} = 0 \tag{3.13}$$

and $K' \geq K$ applies. The inversion of radar backscatter therefore involves the solution of a system of independent linearized integral equations. The solutions to (3.13) reveal that for Doppler frequencies close to the Bragg line, the wave-vector

$\mathbf{K}'$ of the shorter scattering ocean wave is approximately equal to the Bragg wave-vector. These waves normally lie in the saturated region of the ocean wave spectrum. Therefore, in the regions close to the Bragg lines, (3.12) is quasi-linear, since the almost constant short wave may be removed from the integral, which then depends on the long wave component only.

In the Wyatt (1990) approach, the short-wave spectrum $S(K',\alpha')$ is assumed to be the local wind-driven part of the ocean wave spectrum which is assumed to have the shape of Pierson-Moskowitz wind-wave spectrum. Eq. (3.12) then takes the form

$$\sigma_{(2)}(\eta,\phi,D) = \sum_{m,m'=\pm 1} \int_{-\pi}^{\pi} G(K,\alpha) S(K,\alpha) d\theta \tag{3.14}$$

The kernel function, $G(K,\alpha)$, contains the short-wave spectrum $S(K',\alpha')$, the Jacobian J_t, the coupling coefficient γ_t, and scaling terms. The iteration initializes the spectrum by $S(K',\alpha')$ and then progressively adjusts the values at long wavelengths ($S(K,\alpha)$) until, when substituted into (3.14) and integrated, the difference between the integrated and the measured Doppler spectrum is sufficiently small depending on suitable convergence criteria. This method provides estimates of $S(K,\alpha)$ on an irregular wave-number grid. This spectrum is converted to the directional frequency spectrum $E(f,\alpha)$ by using the shallow-water dispersion relationship and then averaged onto a uniform grid:

$$S(K,\alpha) = TE(K,\alpha) \tag{3.15}$$

where

$$T = \frac{g(2k_r)^{\frac{5}{2}}(\tanh(KD) + KD\,\mathrm{sech}^2(KD))}{4\pi K\sqrt{gK\tanh(KD)}} \tag{3.16}$$

and

$$f = \frac{\sqrt{g(2k_r)K\tanh(KD)}}{2\pi}. \tag{3.17}$$

For this study, Wyatt (1990) method was implemented in the processing of six-day WERA data by Seaview Sensing Ltd to get the directional frequency spectra $E(f,\alpha)$.

Chapter 4 Results and Discussions

This chapter will present a comparison of significant wave heights and directional wave spectra between two Tri-Axys buoys and two WERA radars. On the comparison of directional wave spectra, the corresponding results from SWAN model will also be presented. Moreover, this chapter will provide discussions on the WERA data quality on wave measurement. This chapter is organized as follows. Section 4.1 will provide the comparisons of significant wave height. Section 4.2 will present the comparisons of directional wave spectra. Section 4.3 will discuss these results and give some possible reasons for disagreement between Tri-Axys buoys and WERA radars.

4.1 Significant Wave Height (H_s) Comparison

In this thesis, six days of HF WERA data, from 5 to 10 April, 2005, were processed using the algorithm developed by Seaview Sensing Ltd based on Wyatt (1990) to derive wave information. In addition, the two Tri-Axys buoys' data were analyzed for the same period (YD 95-100) to obtain wave parameters and directional wave spectra (Work, 2008). Over the region with sufficient overlapping between the two WERA stations (Figure 2.1), there are over 1,000 WERA cells with surface wave measurements. Here, thirty-three cells have been used to derive wave information to compare with buoy data (Figure 4.1), where these cells are basically

on the cross-shelf transects (i.e., perpendicular to the Florida coastline). The two Tri-Axys buoys were deployed close to the coastline.

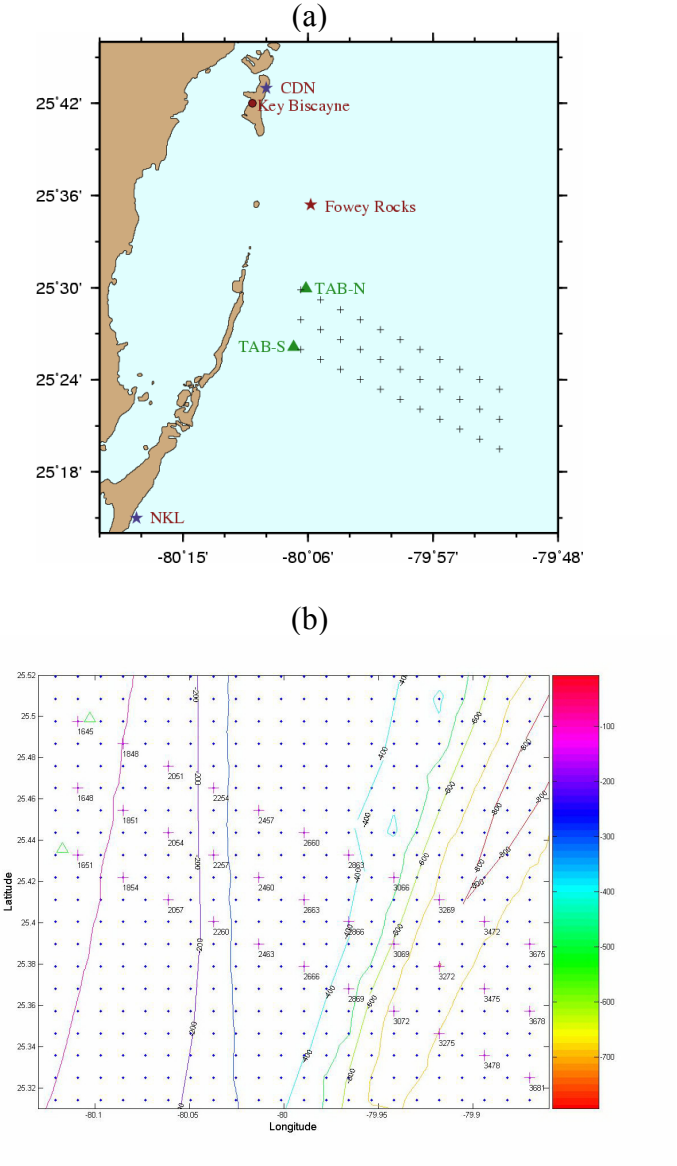

Figure 4.1. (a) Map of the measurement region showing 2 WERA radars and 2 Tri-Axys buoys and Fowey Rocks NDBC CMAN station tower and all used WERA cells. The positions are -80.1052 W in longitude, 25.4991 N in latitude for TAB01041 (TAB-N) and -80.1170 W in longitude, 25.4358 N in latitude for TAB00651 (TAB-S). (b) Expanded view of locations for 33 WERA cells and 2 Tri-Axys buoys. All the available WERA cells are marked with blue point (●).All the 33 cells used for the comparison are marked with magenta cross (+). The positions for two Tri-Axys buoys are marked as green triangles (Δ). The upper triangle is for Tri-Axys buoy TAB-N and the lower one is for TAB-S. The contours and color scales stand for water depths.

The significant wave height H_s has been obtained by integrating the directional wave spectra over the entire direction range and the selected frequency band as described in Eq. (2.1). Figure 4.2 shows the comparison results of the significant wave heights on 8 WERA cells along the line of TAB-N with those from the two Tri-Axys buoys.

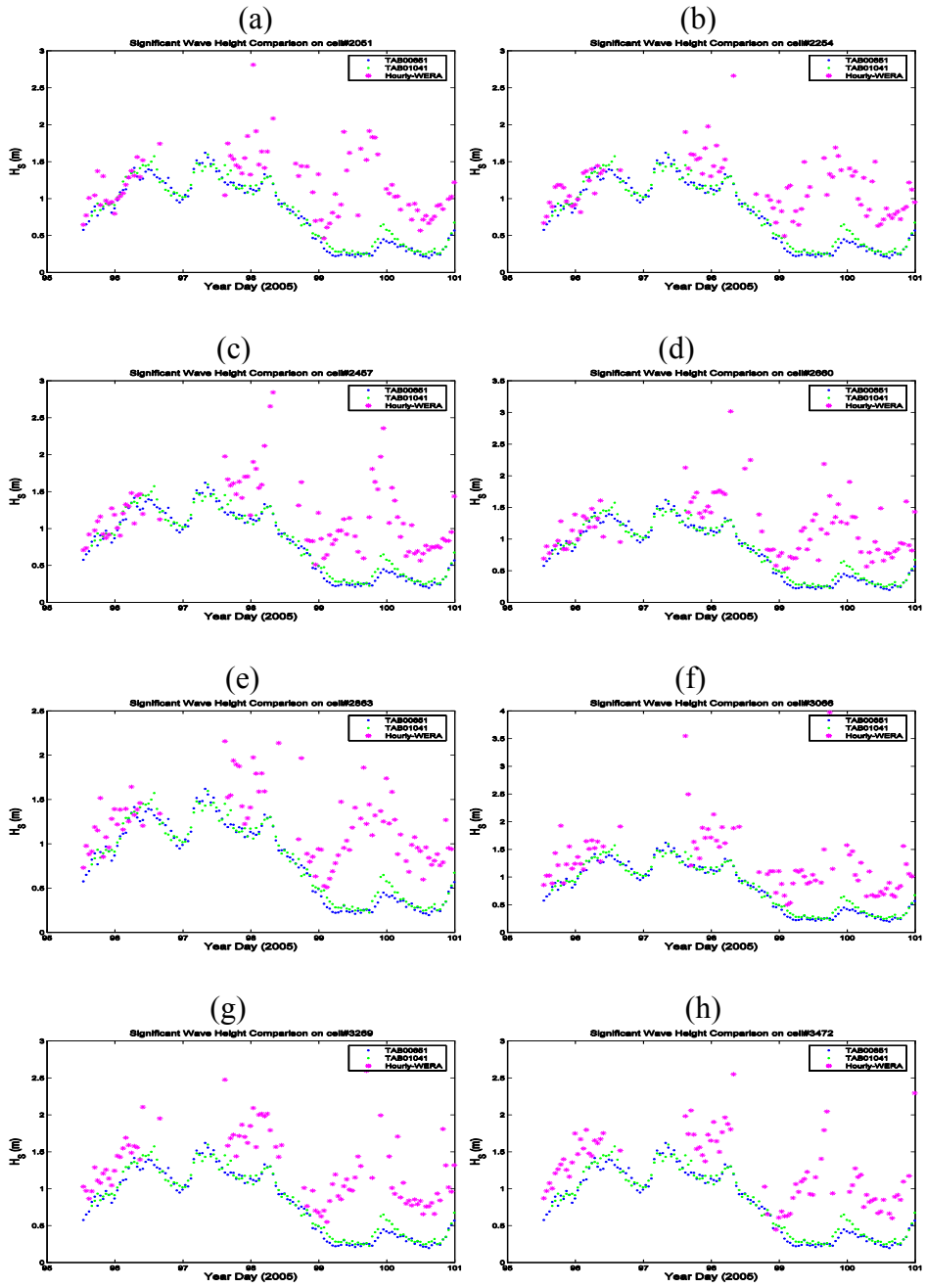

Figure. 4.2. Significant wave heights along the line with TAB01041. (a)-(h) are the results for WERA cell# 2051, 2254, 2457, 2660, 2863, 3066, 3269 and 3472, respectively. The significant wave height measurements from TAB01041 are marked with green points (•). The significant wave height measurements from TAB00651 are marked with blue points (•). Hourly-averaged significant wave height measurements from WERA are marked with magenta star (*).

The two Tri-Axys buoys have a generally good agreement for H_s measurement except for some minor differences: the correlation coefficient between these two buoys significant wave height measurements is $R = 0.9839$. The distance between these two buoys is about 7.2 km in the along-shelf direction. For the comparison results between WERA cells and two Tri-Axys buoys, there are some times with good agreement and other times with which WERA radars have a higher significant wave height measurement than two Tri-Axys buoys. From 1300 GMT, YD 95 to 0700 GMT, YD 96, even though there are some fluctuations of WERA measurements around buoy observations, the comparison agrees well generally except that there is overestimation by cell 3472. There is a gap from 0700 GMT, YD 96 to 1500 GMT, YD 97 in which there is no WERA wave data available. During this period, one of the two WERA radars (NKL WERA site) didn't collect data. Since Wyatt (1990)'s method requires dual-radar measurements available at the same time, there is no wave information retrieved during this time. From 1500 GMT, YD 97 to 0000 GMT, YD 101, the end of the comparison period, the comparison does not agree well: WERA has an overestimation all the time especially during low sea-states (low significant wave height). During the period from YD 99 to YD 100, the significant wave height observations from two Tri-Axys buoys are lower than 1 m, and they are lower than 0.5 m for most of the time. However, the WERA retrieved significant wave heights are much higher than 0.5 m where they range between 1m and 1.5 m.

4.2 Directional Wave Spectrum Comparison

Directional wave spectra from two WERA radars were analyzed by Seaview Sensing Ltd for 6 days, from 5 to 10 April, 2005. Also at the same period, the directional wave spectra from two Tri-Axys buoys were analyzed (Work, 2008). Directional wave spectra calculated by SWAN model are shown in this section to interpret the comparison results between WERA radars and Tri-Axys buoys. Like the comparison results on the significant wave height H_s, the comparison results on the directional wave spectra show that there are some times of good agreement and other times of disparity. The wind data are obtained from the NDBC station FWYF1, Fowey Rocks, FL. The NDBC tower is about 17.5 km from one of the Tri-Axys buoys TAB00651.

Directional wave spectra between WERA, TAB00651 and SWAN model are shown in Figure 4.3 and 4.4. This selected WERA cell 2257 is about 8.9 km from TAB00651. There is disagreement between directional wave spectra at cell 2257 and TAB00651 and SWAN model (Figure 4.3). The wind direction obtained from Fowey Rocks tower is 96.3^{o} clockwise from the north and the wind speed is 6 ms^{-1}. The WERA spectrum (Figure 4.3.a) doesn't show any wave propagating in this direction. Instead, it shows a wave system with peak period 7.2 s propagating to the south. The WERA observation was taken on 1315 GMT, YD 95. The buoy observation from TAB00651 was taken after 35 minutes, and it did show some waves propagating along the wind direction, though there were the other lower frequency waves propagating along the south-west direction (Figure 4.3.b). SWAN

model was taken on 1300 GMT, YD 95 (Figure 4.3.c). The model was run on the region covering WERA wave measurement region. The model cell selected here is close to the WERA cell 2257. The model result showed one wave system propagating along the wind direction with a lower energy level than buoy result.

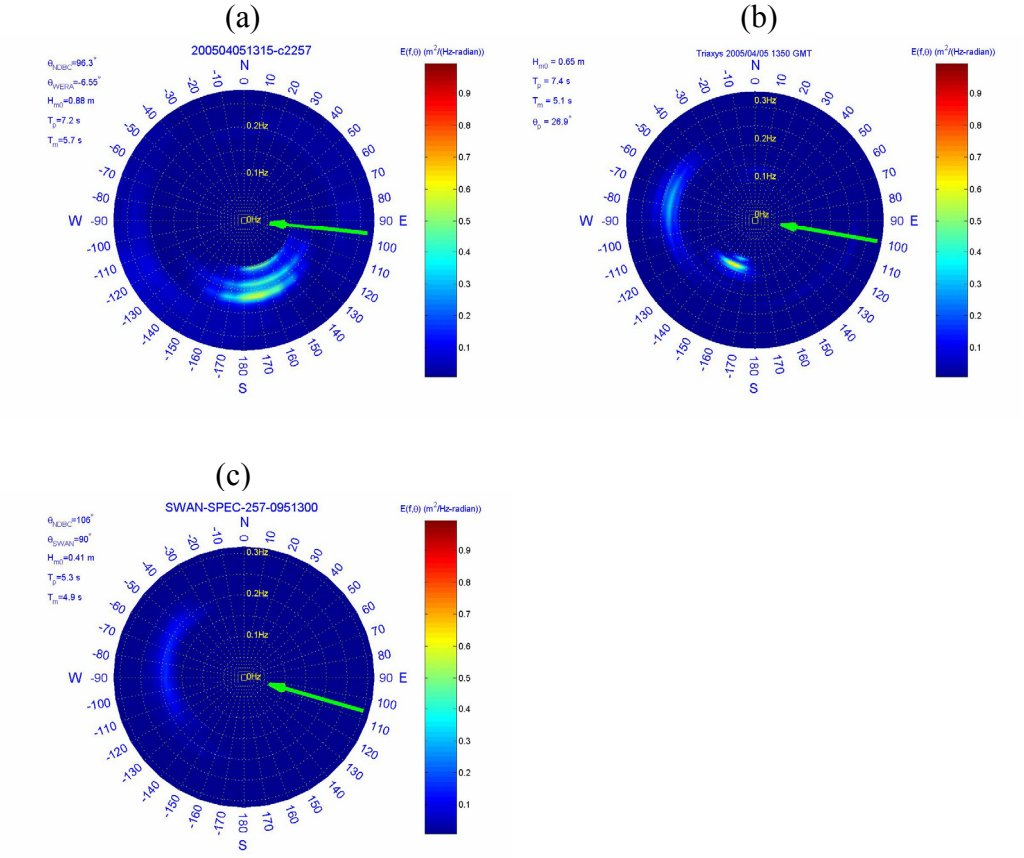

Figure 4.3 Directional wave spectra. Figure (a) is for WERA cell 2257 taken on 1315 GMT, YD 95; figure (b) is for TAB00651 taken on 1350 GMT, YD 95; figure (c) is for SWAN model cell close to WERA cell 2257 taken on 1300 GMT, YD 95. For all three figures, the green arrows represent wind direction from which it comes. The wind information is obtained from Fowey Rocks NDBC tower. The selected WERA cell 2257 is located -80.04 W in longitude and 25.43 N in latitude.

Directional wave spectra are shown for another different time from the same WERA cell 2257 in Figure 4.4. Generally, the comparison agrees well between WERA, buoy and SWAN model. At this time, the wind direction from Fowey Rocks was 85.1^{o} clockwise from the north with a wind speed of 9.2 ms^{-1}. The WERA directional wave spectrum was taken on 0245 GMT, YD 96. The WERA retrieved wind direction is 72^{o} clockwise from the north, the significant wave height is 1.3 m with a peak period 4.7 s. This represents wave with a frequency of approximately 0.2 Hz (Figure 4.4.a). The buoy directional wave spectrum was taken on 0250 GMT, YD 96. The buoy retrieved wind direction is 98.9^{o} clockwise from the north, the significant wave height is 1.1m and the peak period is 5.4 s (Figure 4.4.b). The directional wave spectrum from the model was taken on 0300 GMT, YD 96. For an input wind direction of 106^{o} clockwise from the north, the corresponding significant wave height is 0.98 m and the peak wave period is 6.7 s (Figure 4.4.c). The wind field used here differs for WERA, TAB00651 and SWAN, for example, the SWAN input wind is hourly-averaging wind field obtained from Fowey Rocks C-MAN station, while the wind field used for TAB00651 and WERA is 10-minute-averaging wind from the same tower.

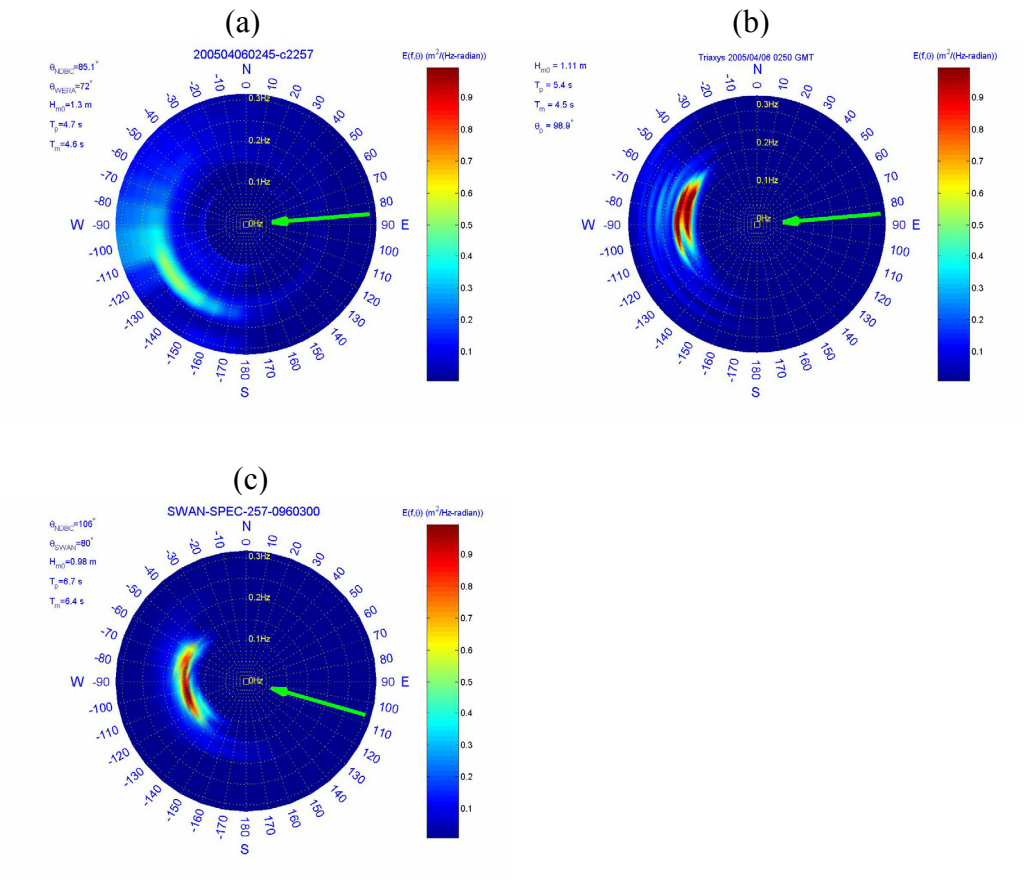

Figure 4.4 Directional wave spectra. Figure (a) is for WERA cell 2257 taken on 0245 GMT, YD 96; figure (b) is for TAB00651 taken on 0250 GMT, YD 96; figure (c) is for SWAN model cell close to WERA cell 2257 taken on 0300 GMT, YD 96. For all three figures, the green arrows represent wind direction from which it comes. The wind information is obtained from Fowey Rocks NDBC tower.

Directional wave spectra for another WERA cell at the same time as Figure 4.4 are shown in Figure 4.5. This cell (# 2866) is further offshore than cell 2257 (Figure 4.1.b). The SWAN model cell used here is close to this WERA cell, and the comparison suggests reasonable agreement between WERA, buoy and SWAN model. Wind direction from Fowey Rocks was 85.1^{o} clockwise from the north with a wind speed of 9.2 ms^{-1}. The WERA directional spectrum was taken on 0245 GMT, YD 96. The retrieved wind direction is 65.5^{o} clockwise from the north, the significant wave height is 1.2 m and the peak period is 4.9 s (wave frequency of 0.2

Hz) (Figure 4.5.a). The buoy retrieved wind direction is 98.9^{o} clockwise from the north, the significant wave height is 1.11m and the peak period is 5.4 s (see Figure 4.4.b). The SWAN model input wind direction is 106^{o} clockwise from the north, the significant wave height is 0.99 m and the peak wave period is 6.7 s (Figure 4.5.b).

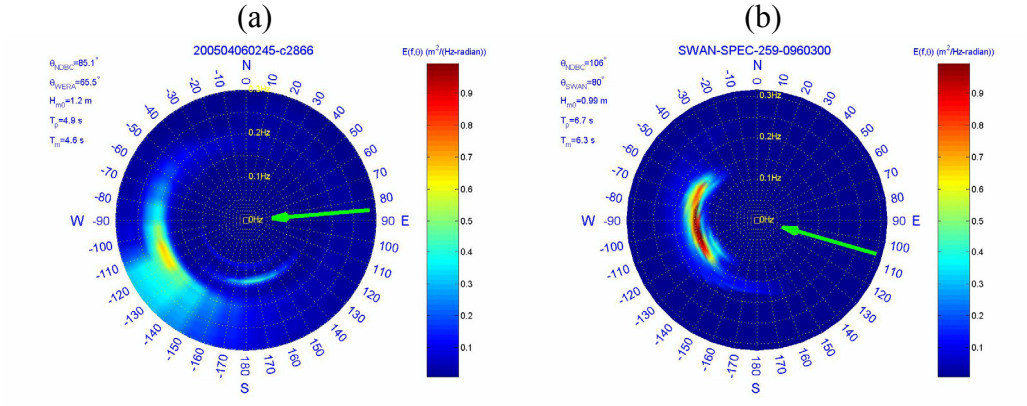

Figure 4.5 Directional wave spectra. Figure (a) is for WERA cell 2866 taken on 0245 GMT, YD 96; figure (b) is for SWAN model cell close to WERA cell 2866 taken on 0300 GMT, YD 96. For these two figures, the green arrows represent wind direction from which it comes. The wind information is obtained from Fowey Rocks NDBC tower.

Directional wave spectra for another WERA cell on the same time as Figure 4.4 are shown in Figure 4.6. This WERA cell (cell # 3475) is further offshore than cell 2866 (Figure 4.1.b).The SWAN model cell used here is close to this WERA cell. Generally, the comparison agrees well between WERA, buoy and SWAN model. The wind direction from Fowey Rocks was 85.1^{o} clockwise from the north and the wind speed was 9.2 ms^{-1}. The WERA directional spectrum was taken on 0245 GMT, YD 96. The WERA retrieved wind direction is 65.5^{o} clockwise from the north, the significant wave height is 1.6 m with a peak period of 5.5 s (Figure 4.6.a). The buoy retrieved wind direction is 98.9^{o} clockwise from the north, the significant wave

height is 1.11m with a peak period of 5.4 s (see Figure 4.4.b). The SWAN model input wind direction is 106^{o} clockwise from the north, the significant wave height is 0.99 m and the peak wave period is 6.7 s (Figure 4.6.b).

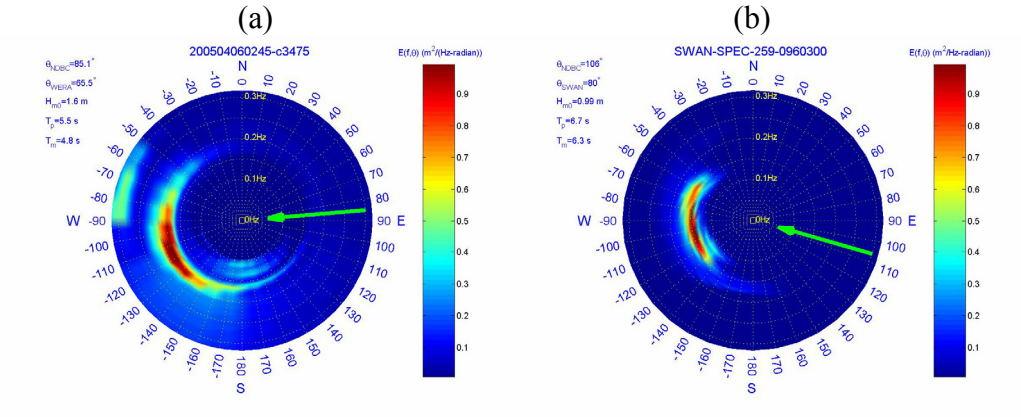

Figure 4.6 Directional wave spectra. Figure (a) is for WERA cell 3475 taken on 0245 GMT, YD 96; figure (b) is for SWAN model cell close to WERA cell 2866 taken on 0300 GMT, YD 96. For these two figures, the green arrows represent wind direction from which it comes. The wind information is obtained from Fowey Rocks NDBC tower.

4.3 Discussions

Generally, there is general agreement on the comparison of significant wave height and directional wave spectrum between WERA measurements and buoy observations. However, the comparison does not agree well all the time. There are some possible reasons for this disagreement.

First, noise related issues can be caused by radar antenna side-lobe contamination or RFI (Radio Frequency Interference). The sampling times for WERA wave measurements were too short. For the need to provide updated currents at 20-minute intervals and to reduce data storage requirement, each of two radar

observations was derived from a 5-minute (1024 samples) transmit/receive window. The five minute interval was insufficient to reduce antenna side-lobe noise adequately. When there is higher-noise level in echo-Doppler spectrum, the retrieved directional wave spectrum has a higher energy level since wave retrieval from WERA needs the 2nd-order Bragg scattering. During the low sea-states, the noise level is high and is even higher than the 2nd-order sidebands at times. The noise level has blurred the 2nd-order backscattered power and brought spurious energy into directional wave spectrum retrieval. On the retrieved WERA directional wave spectrum, this high noise contamination induces spurious waves in the directional spectrum (Figure 4.3.a). These directional wave spectra result in higher significant wave height H_s retrieval obtained by integrating the directional wave spectrum over the entire direction range and the selected frequency band. Moreover, HF radar observations are sensitive to radio frequency interference (RFI), which likely causes the high-noise level in the sampling. RFI can degrade the data quality of HF radar measurements. The typical structure of RFI consists of vertical lines, extending all over radar resolution ranges. It can contaminate the backscattered echo and induce pseudo-high signal to the backscattered Doppler spectra, therefore will affect the quality of the measurements. For the WERA phased-array radar, the wave measurements are more sensitive to RFI than current measurements due to the lower signal-to-noise ratio (SNR) of the 2nd-order returns used for wave measurements.

When there was low noise in the echo-Doppler spectrum (Figure 4.7), there wave a good retrieval of significant wave height. The Doppler spectra were obtained

from two WERA sites: CDN site and NKL site and averaged hourly, respectively. These Doppler spectra were taken on WERA cell 2051 (Figure 4.1.b). Where the upper spectrum was obtained from WERA CDN site and the lower spectrum was taken from WERA NKL site. This cell 2051 is about 5.6 km away from TAB01041 and 7.7 km from TAB00651. Over this time, the agreement between buoy and WERA measurements is considered good. The H_s observations at this time are 0.91 m from TAB01041 and 0.84 m from TAB00651, and the retrieved H_s from WERA is 0.91 m. For both Doppler spectra, the noise level is low. For example, the noise level is below 35 dB for the CDN site and is below 30 dB for the NKL site. In addition, the 2nd-order sidebands from both of the radar sites are obvious where the higher 2nd-order sideband peak is 59 dB for the CDN site and is 52 dB for the NKL site. Therefore, the corresponding 2nd-order SNR is above 24 dB for the CDN site and above 22 dB for the NKL site. Wyatt (1990)'s method sets 15 dB as a criteria for 2nd-order SNR. These two Doppler spectra meet this criteria and can get good results on wave retrieval.

An echo-Doppler spectrum with higher noise level from both of the radar site is shown in Figure 4.8. The Doppler spectra were obtained on 1930 GMT, YD 99. The H_s observations at this time are 0.41 m from TAB01041 and 0.29 m from TAB00651, however, the retrieved H_s from WERA is 1.83 m, where the noise level is above 40 dB for both of the radar sites. On the CDN Doppler spectrum, we can see the obvious 2nd-order Bragg side-band close to the higher 1st-order Bragg peak, however, we can't see the expected 2nd-order Bragg side-band on the NKL Doppler spectrum. Since Wyatt's method (1990) requires dual-radar measurement, the bad

Doppler spectrum from one of the radar site means poor 2nd-order SNR from this site. The NKL Doppler spectrum indicates that the noise level is the same as the 2nd-order side-bands. Since the wave measurement requires high 2nd-order SNR ratio, the H_s retrieval on this cell is not good. However, the 1st-order Doppler peaks are still easily observed even with this strong noise effect from these two radar sites. An example on bad retrieval of significant wave height from two radar sites is shown in Figure 4.8. It was the case for the entire period from 1500 GMT, YD 97 to 0000 GMT, YD 101, which is one possible reason for poor comparison result between buoy and radar observations. Figure 4.9 shows another example of Doppler spectra on bad retrieval of significant wave height from two radar sites. The echo-Doppler spectra were obtained on 2330 GMT, YD 100, 2005. The H_s observations at this time are 0.67 m from TAB01041 and 0.57 m from TAB00651, however, the retrieved H_s from WERA is nearly double with a value of 1.22 m.

Additionally, comparison of significant wave height between two WERA radars and Sontek buoy are shown in Figure 4.10. The WERA retrieved significant wave heights differ from those used in this study. They are not obtained by integrating the directional wave spectra, instead they are obtained by an empirical method (Ramos, 2006). The empirical method of Ramos (2006) uses the ratio between the 2nd-order peaks, scaled by a weighting function (Barrick, 1977) to define the directionally integrated wave parameter H_s. As shown in Figure 4.10, it has a generally good agreement between two radars and Sontek buoy. In the low sea-states, the comparison results don't show overestimation from WERA radar measurements. The H_s comparisons were for cells close to the radar look-direction where side-lobe effects

were minimized. The directional spectra could only be obtained in regions with large angles to the radar look-direction because of the overlapping requirement. This makes the results more sensitive to side-lobe effects and RFI. It turns out that this noise issue must be resolved before integrating the directional wave spectrum to obtain the better significant wave height measurements.

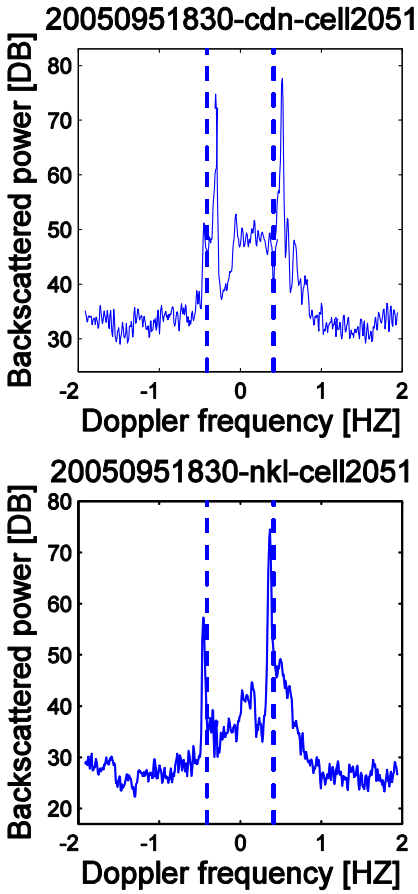

Figure 4.7. Echo-Doppler spectra on WERA cell 2051 from both WERA sites. The solid lines represent the backscattered power and the dashed lines represent the Bragg frequencies (For WERA carrier frequency 16.045 MHz, the Bragg frequencies are ± 0.41 Hz.). The Doppler spectra were averaged hourly. The upper figure represents the Doppler spectrum obtained from CDN WERA site and the lower one stands for NKL WERA site. The obtained time is 1830 GMT, YD 95, 2005.

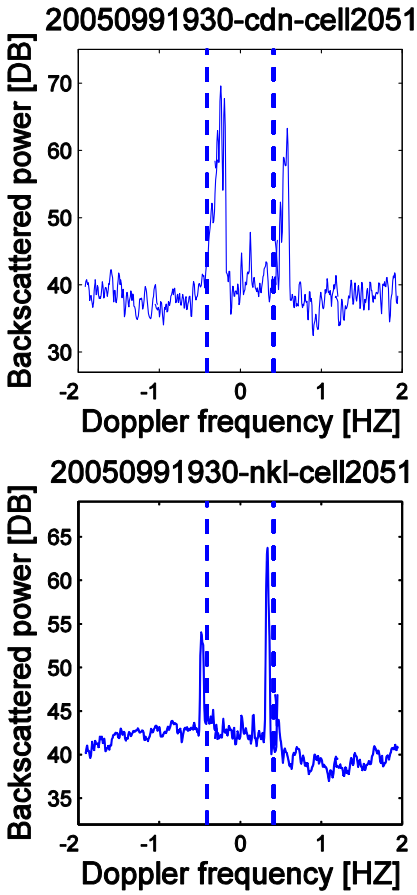

Figure 4.8. Echo-Doppler spectra on WERA cell 2051 from both WERA sites. The solid lines represent the backscattered power and the dashed lines represent the Bragg frequencies (For WERA carrier frequency 16.045 MHz, the Bragg frequencies are ± 0.41 Hz.). The Doppler spectra were averaged hourly. The upper figure stands for the Doppler spectrum obtained from CDN WERA site and the lower one stands for NKL WERA site. The obtained time is 1930 GMT, YD 100, 2005.

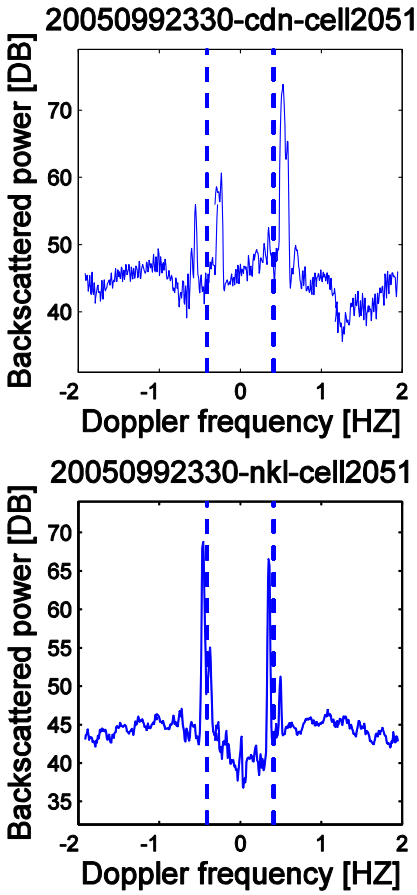

Figure 4.9. Echo-Doppler spectrums on WERA cell 2051 from both WERA sites. The solid lines represent the backscattered power and the dashed lines represent the Bragg frequencies (For WERA carrier frequency 16.045 MHz, the Bragg frequencies are ± 0.41 Hz.). The Doppler spectra were averaged hourly. The upper figure stands for the Doppler spectrum obtained from CDN WERA site and the lower one stands for NKL WERA site. The Obtained time is 2330 GMT, YD 100, 2005.

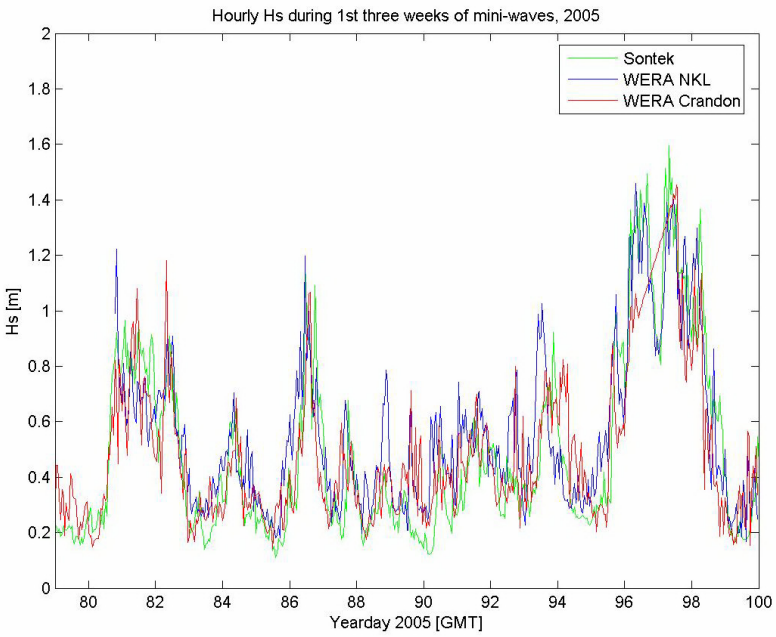

Figure. 4.10. Comparison results of significant wave height between two WERA radars and Sontek.

The second possible reason is the spatial variability of horizontal current shear. The Florida Strait is under the effect of the Florida Current, which has strong horizontal current shear. The study area for this thesis is also under the effect of the Florida Current (Figure 4.11). The current field was obtained from WERA current measurements and was taken on 0300 GMT, YD 96. At this time, from the radar cell close to shore (cell # 2257), the WERA retrieved wind direction was 72^{o} and the buoy retrieved wind direction was 98.9^{o} clockwise from the north. The wind direction obtained from Fowey Rocks tower was 85^{o} clockwise from the north (Figure 4.4 (a) and (b)). Compared with the Fowey Rocks tower wind direction, the WERA retrieved wind direction differed by approximately 13^{o} to the left. From the WERA cells further offshore (cell # 2866 and cell # 3475), the WERA retrieved wind direction was 65.5^{o} clockwise from the north (Figure 4.5a and Figure 4.6 a).

Compared with the Fowey Rocks tower wind direction, the WERA retrieved wind direction deviated about 19.5^{o} to the left. This direction deviation can result from the horizontal current shear of Florida Current. Kenyon (1971) presented that following (opposing) waves travelling over a sheared current would be refracted in the direction of decreasing (increasing) current field. The WERA cell 2257, 2866 and 3475 are in the region under the effect of the horizontal current shear variability (Figure 4.11). The wind blew to the Florida coast, with the southward component which was against the direction of Florida Current (Figure 4.4a, Figure 4.5a, Figure 4.6a). In that case, the wave would be refracted in the direction of increasing current field. The current (and shear) field was stronger on cell 3475 than on cell 2257, which induced more wave propagation direction deviation. As shown in Figure 4.12, Florida Current has an effect on SWAN model results also. Without current present, the retrieved wind direction from SWAN is 90^{o} clockwise from the north, while it is 80^{o} clockwise from the north with current input.

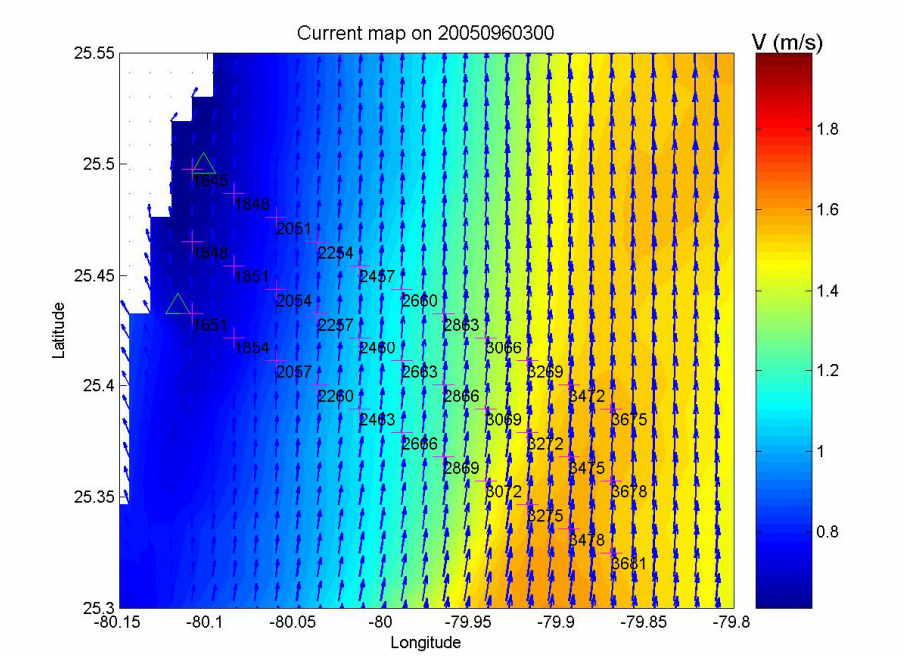

Figure 4.11 Current field on 0300 GMT, YD 96. The color represents the current magnitude and the arrow means the current direction. All the 33 cells are shown in + and the two Tri-Axys buoys are shown in Δ.

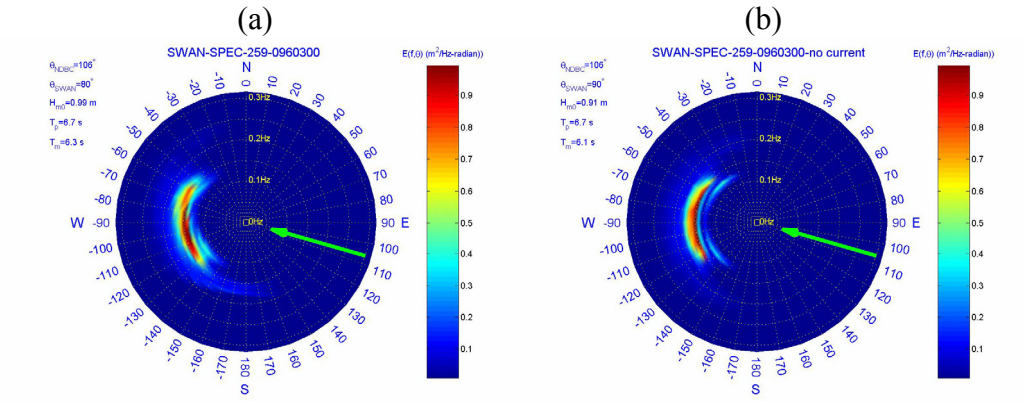

Figure 4.12 Directional wave spectra. Figure (a) is for SWAN model taken on 0300 GMT, YD 96, figure (b) is for SWAN model without current input at the same time. For these two figures, the green arrows represent wind direction from which it comes. The wind information is obtained from Fowey Rocks NDBC tower.

Chapter 5 Summary

The study of surface waves plays an important role on marine-related research which ranges from sea-state forecasts, oceanographic and fisheries research, vessel navigation safety, and the planning and operation of oceanic engineering projects. From this perspective, reliable and economic real-time monitoring of ocean surface wave field is of considerable interest and importance.

Buoys are a traditional tool to measure surface waves and can provide reliable wave measurements. These measurements can provide large quantities of wave data at a fixed point. However, buoys are susceptible to theft, vandalism and damage from shipping; they could be overturned by steep breaking waves too. Moreover, buoys don't work well in regions with strong currents, such as the region along the Florida Current. Thus, it is not reasonable to deploy many buoys on the area of interest due to high expenses to maintain them.

Due to these disadvantages of buoy wave measurements, it is useful to utilize remote-sensing techniques. In this region, the high-frequency radar technology is an ideal ground-based remote sensing tool that can measure both directional wave spectra and surface currents over a wide area of the coastal ocean. To establish the credibility of HF radar wave measurements, detailed comparisons with buoys are required to ensure that the radar wave data are of high quality and reliability. For this objective, an experiment, called Mini-Waves experiment was conducted from March to May, 2005 on the WERA footprint along the southeast Florida coast where two Tri-Axys were deployed during this period (Voulgaris et al, 2008).

In this thesis, six days data of backscattered returns from two WERA radars were used to estimate surface waves that were then compared to Tri-Axys buoys. Results on the significant wave height and directional wave spectra are presented. When the wind blew onshore and was steady for several hours, the significant wave height measurements from WERA radars agreed well with those from Tri-Axys buoys. However, when the wind changed in magnitude and direction over a short period, especially during the low sea-states, the significant wave height measurements from WERA didn't agree well with those from buoys. In general, WERA measurements overestimated the significant wave height measurements. Moreover, for the comparison of the directional wave spectra, SWAN model results were used to verify the comparison results between buoys and WERA radars. Generally, there is good agreement on the comparison results between buoys and SWAN model. The agreement between WERA and buoys is good for some times and bad for the other times.

There are several possible reasons for this disagreement. The first reason is noise issue caused by antenna side-lobe contamination or RFI on the echo-Doppler spectrum during low sea states. It will bring spurious energy to the directional wave spectrum retrieval and cause higher significant wave height measurements. The second possible reason is that the study area is under the effect of the horizontal current shear of Florida current. The spatial variability of current shear can cause the deviation of wave propagation direction.

To improve the data quality from WERA wave measurements, the sampling method for the WERA observations was changed in 2006 from 5-minute intervals (1024 samples) to 10-minute intervals (2048 samples) from each radar site. This

longer averaging can provide improved spectral noise suppression. Additionally, two steps were implemented to suppress RFI effect on WERA observations. The first step is to apply an automatic frequency scan just before a measurement cycle starts and to calculate the best frequency range for the next measurement cycle and to adjust the WERA control file. The second step is to apply a RFI suppression algorithm and to get the information on the structure of the actual RFI within the measurement. This information can be utilized to calculate a spectral filter to remove most of the RFI from the backscattered Doppler spectrum. Moreover, two new WERA sites have been deployed in Dania Beach and Virginia Key Beach, which can provide wider overlapping area for wave measurements. In addition, in-situ measurements are required to evaluate the feasibility of these changes, particularly concerning the wave measurement from WERA HF radars since the wave measurements are more sensitive to short sampling intervals and RFI than current measurements.

References:

Atanga, J. N. and L. R. Wyatt, 1997: Comparison of inversion algorithms for HF radar wave measurements, *IEEE Journal of Oceanic Engineering*, **22 (4)**, 593-603.

Barrick, D. E., 1972a: First-order theory and analysis of MF/HF/VHF scatter from the sea, *IEEE Trans. Antennas Propag.*, **20**, 2-10

Barrick, D. E., 1972b: Remote sensing of sea state by radar, Chapter 12 of *Remote Sensing of the Troposphere*, V.E. Derr, Editor, NOAA/Environmental Research Laboratories, Boulder, CO, 186-192.

Barrick, D. E., M. W. Evans and B. L. Weber, 1977a: Ocean surface currents mapped by radar, *Science*, **198**, 138-144.

Barrick, D. E., 1977b: Extraction of wave parameters from measured HF radar sea-echo Doppler spectra, *Radio Science*, **12 (3)**, 415-424.

Bathgate, J. S., M. L. Heron and A. Prytz, 2006: A method of swell-wave parameter extraction from HF ocean surface radar spectra, *IEEE Journal of Oceanic Engineering*, **31 (4)**, 812-818.

Chapman, R. D., L. K. Shay, H. C. Graber, J. B. Edson, A. Karachintsev, C. L. Trump and D. B. Ross, 1997: On the accuracy of HF radar surface current measurement: intercomparisons with ship-based sensors, *Journal of Geophysical Research*, **102 (C8)**, 18,737-18,748.

Crombie, D. D., 1955: Doppler spectrum of sea echo at 13.56 Mc/s, *Nature*, **175**, 681-682.

Donelan, M. A., J. Hamilton and W. H. Hui, 1985: Directional spectra of wind-generated waves, *Phil. Trans. R.. Soc. Lond. A*, **315**, 509-562.

Donelan, M., 1990: Air-sea interaction, chapter in *The Sea* – Vol (9): Ocean Engineering Science. B. LeMahaute and D. M. Hanes (Eds.). Wiley Interscience, 239-292.

Donelan, M. A., M. Skafel, H. C. Graber, P. Liu, D. Schwab and S. Venkatesh, 1992: On the growth rate of wind-generated waves, *Atmosphere-Ocean*, **30 (3)**, 457-478.

Donelan, M. A., B. K. Haus, N. Reul, W. J. Plant, M. Stiassnie, H. C. Graber, O. B. Brown and E. S. Saltzman, 2004: On the limiting aerodynamic roughness of the ocean in very strong winds, *Geophysical Research Letters*, **31**, L18306,doi:10.1029/2004GL019460.

Essen, H. H., K. W. Gurgel and T. Schlick, 1999: Measurement of ocean wave height and direction by means of HF radar: an empirical approach, *Dt. Hydorgr. Z.*, **51**, 369-383.

Ewans, K. C., 1997: Observations of the directional spectrum of fetch-limited waves, *Journal of Physical Oceanography*, **28**, 495-512.

Gill, Eric, W. Huang and J. Walsh, 2006: On the development of a second-order bistatic radar cross section of the ocean surface: a high-frequency result for a finite scattering patch, *IEEE Journal of Oceanic Engineering*, **31 (4)**, 740-750.

Graber, H. C., B. K. Haus, R. D. Chapman and L. K. Shay, 1997: HF radar comparisons with moored estimates of current speed and direction: expected differences and implications, *Journal of Geophysical Research*, **102 (C8)**, 18,749-18,766.

Gurgel, K. W. and G. Antonischki, 1997: Remote sensing of surface currents and waves by the HF radar WERA, *7th international conference on electronic engineering in oceanography*, 23-25 June, 211-217.

Gurgel, K. W., H. H. Essen and S. P. Kingsley, 1999a: High-frequency radars: physical limitations and recent developments, *Coastal Engineering*, **37**, 201-218.

Gurgel, K. W., G. Antonischki, H. H. Essen and T. Schlick, 1999b: Wellen Radar (WERA): a new ground-wave HF radar for ocean remote sensing, *Coastal Engineering*, **37**, 219-234.

Gurgel, K. W. and T. Schlick, 2005: HF radar wave measurements in the presence of ship echoes: problems and solutions, *Oceans-Europe*, 937-941.

Gurgel, K. W., 2005: HF radar in oceanography: advantages and limitations, Presentation on RSMAS MPO seminar series, Fall, 2005.

Gurgel, K. W., H. H. Essen and T. Schlick, 2006: An empirical method to derive ocean waves from second-order Bragg scattering: prospects and limitations, *IEEE Journal of Oceanic Engineering*, **31 (4)**, 804-811.

Hashimoto, N. and M. Tokuda, 1999: A Bayesian approach for estimation of directional wave spectra with HF radar, *Coastal Engineering*, **41 (2)**, 137-149.

Hasselmann, K., 1971: Determination of ocean wave spectra from Doppler radio return from the sea surface, *Nature Physical Science*, **229**, 16-17.

Haus, B. K., R. J. Ramos, H. C. Graber, L. K. Shay and Z. R. Hallock, 2006: Remote observation of the spatial variability of surface waves interacting with an estuarine outflow, *IEEE Journal of Oceanic Engineering*, **31 (4)**, 835-849.

Haus, B. K., 2007: Surface current effects on the fetch-limited growth of wave energy, *Journal of Geophysical Research*, **112**, C03003, doi:10.1029/2006JC003924.

Heron, M. L., P. E. Dexer and B. T. McGann, 1985: Parameters of the air-sea interface by high-frequency ground-wave Doppler radar, *Aust. J. Mar. Freshw. Res.*, **36**, 655-670.

Hisaki, Y., 1996: Nonlinear inversion of the integral equation to estimate ocean wave spectra from HF radar, *Radio Science*, **31 (1)**, 25-39.

Hisaki, Y., 2005: Ocean wave directional spectra estimation from an HF ocean radar with a single antenna array: observation, *Journal of Geophysical Research*, **110**, C11004, doi:10.1029/2005JC002881.

Hisaki, Y., 2006: Ocean wave directional spectra estimation from an HF ocean radar with a single antenna array: methodology, *Journal of Atmospheric and Oceanic Technology*, **23**, 268-286.

Hisaki, Y., 2007: Directional distribution of the short wave estimated from HF ocean radars", *Journal of Geophysical Research*, **112**, C10014, doi: 10.1029/2007JC004296.

Howell, R. and J. Walsh, 1993: Measurement of ocean wave spectra using narrow-beam HF radar, *IEEE Journal of Oceanic Engineering*, **18 (3)**, 296-305.

Jeans, G., C. Primrose, N. Descusse, S. Strong and P. van Weert, 2003: A comparison between directional wave measurements from the RDI Workhorse with Waves and the Datawell Directional Waverider, *Proc. Of IEEE/OES seventh working conference on current measurement technology*, 148-151.

Jonsson, I. G., 1990: Wave current interactions, *The Sea* Volume 9 B: Ocean Science Engineering, Edited by Bernard LeMehaute and Daniel M. Hanes, John Wiley & Sons, Inc, 65-120.

Kenyon, K. E., 1971: Wave refraction in ocean currents, *Deep-Sea Research*, **18**, 1023-1034.

Kingsley, S. P., A. Matoses and L. R. Wyatt, 1998: Analysis of second order HF radar sea spectra recorded in storm conditions, *IEEE*, 459-462.

Krogstad, H. E., J. Wolf, S. P. Thompson and L. R. Wyatt, 1999: Methods for intercomparison of wave measurements, *Coastal Engineering*, **37**, 235-257.

MacIver, R. D., R. R. Simons and G. P. Thomas, 2006: Gravity waves interacting with a narrow jet-like current, *Journal of Geophysical Research*, **111**, C03009, doi:10.1029/2005JC003030.

Mei, C. C. and C. Benmoussa, 1984: Long waves induced by short-wave groups over an uneven bottom, *Journal Fluid Mech*, **139**, 219-235.

Middleditch, Andrew and L. R. Wyatt, 2006: An instantaneous-frequency filtering technique for high-frequency radar oceanography, *IEEE Journal of Oceanic Engineering*, **31 (4)**, 797-803.

Nadai, Akitsugu, 2006: Model analysis of influence of wave-current interaction on current measurement of HF ocean surface radar for isolated eddy and upwelling, *Journal of Geophysical Research*, **111**, C10012, doi: 1029/2006JC003528.

Paduan, J. D., K. C. Kim, M. S. Cook and F. P. Chavez, 2006: Calibration and validation of direction-finding high-frequency radar ocean surface current observations, *IEEE Journal of Oceanic Engineering*, **31 (4)**, 862-875.

Ramos, R. J., 2006: 2-D analysis of wave energy evolution using wavelet transforms, Ph.D. thesis, Univ. of Miami, Miami, Fla., March.

Phillips, O. M., 1981: The structure of short gravity waves on the ocean surface, *Spaceborne synthetic aperture radar for oceanography*. Baltimore, MD, Johns Hopkins University Press, 24-31.

Shay, L. K., J. M. Pedraja, T. M. Cook, B. K. Haus and R. H. Weisberg, 2007: High-frequency radar mapping of surface currents using WERA, *Journal of Atmospheric and Oceanic Technology*, **24**, 484-503.

Shay, L K., H. Seim, D. Savidge, R. Styles and R. H. Weisbert, 2008: Lessons learned using high frequency radar during the Southeast Atlantic Coastal Ocean Observing System deployment, *Marine Technical Society Journal*, **42(3)**, 55-67..

Trizna, Dennis and Lillian (Xialon) Xu, 2006: Target classification and remote sensing of ocean current shear using a dual-use multifrequency HF radar, *IEEE Journal of Oceanic Engineering*, **31 (4)**, 904-918.

Valk, C., A. Reniers, J. Atanga, A. Vizinho and J. Vogelzang, 1999: Monitoring surface waves in coastal waters by integrating HF radar measurement and modeling, *Coastal Engineering*, **37**, 431-453.

Voulgaris, G., B. K. Haus, P. Work, L. K. Shay, H. Seim, R. H. Weisberg, and J. Nelson, 2008: Waves initiative within SEACOOS, *J. Marine Tech. Society*, **42(3)**, 68-79.

Walsh, E. J., L. K. Shay, H. C. Graber, A. Guillaume, D. Vandemark, D. E. Hines, R. N. Swift and J. F. Scott, 1996: Observations of surface wave-current interaction during SWADE, *The Global Atmosphere and Ocean System*, **5**, 99-124.

Work, P. A., 2008: Nearshore directional wave measurements by surface-following buoy and acoustic Doppler current profiler, *OceanEngineering*, **35 (8-9)**, 727-737.

Wyatt, L. R., 1990: Inversion of the HF radar Doppler spectrum for ocean wave measurement.

Wyatt, L. R., 1990: A relaxation method for integral inversion applied to HF radar measurement of the ocean wave directional spectrum, *International Journal of Remote Sensing*, **11 (8)**, 1481-1494.

Wyatt, L. R., 1991: High-frequency radar measurements of the ocean wave-directional spectrum, *IEEE Journal of Oceanic Engineering*, **16 (1)**, 163-169.

Wyatt, L. R. and G. J. Holden, 1992: Developments in ocean wave measurements by HF radar, *IEE Proceedings-F*, **139 (2)**, 170-174.

Wyatt, L. R., 1995: High order nonlinearities in HF radar backscatter from the ocean surface, *IEE Proc.-Radar, Sonar Navig.*, **142 (6)**, 293-300.

Wyatt, L. R., L. J. Ledgard and C. W. Anderson, 1997: Maximun-likelihood estimation of the directional distribution of 0.53 Hz ocean waves, *Journal of Atmospheric and Oceanic Technology*, **14**, 591-603.
Wyatt, L. R., 1998: HF radar wave measurement in high sea-states, *IEEE*, 463-466.

Wyatt, L. R., S. P. Thompson and R. R. Burton, 1999: Evaluation of high frequency radar wave measurement, *Coastal Engineering*, **37**, 259-282.

Wyatt, L. R., 2000: Limits to the inversion of HF radar backscatter from ocean wave measurement, *Journal of Atmospheric and Oceanic Technology*, **17**, 1651-1666.

Wyatt, L. R. and J. J. Green, 2002: The availability and accuracy of HF radar wave measurements, *IEEE*, 515-517.

Wyatt, L. R., J. J. Green, K. W. Gurgel, J. C. Nieto Borge, K. Reichert, K. Hessener, H. Gunther, W. Rosenthal, O. Saetra and M. Reistad, 2003: Validation and intercomparison of wave measurements and models during the EuroROSE experiments, *Coastal Engineering*, **48**, 1-28.

Wyatt, L. R., G. Liakhovetski, H. C. Graber and B. K. Haus, 2005: Factors affecting the accuracy of SHOWEX HF radar wave measurements, *Journal of Atmospheric and Oceanic Technology*, **22**, 847-859.

Wyatt, L. R., J. J. Green, A. Middleditch, M. D. Moorhead, J. Howarth, M. Holt and S. Keogy, 2006: Operational wave, current, and wind measurements with the Pisces HF radar, *IEEE Journal of Oceanic Engineering*, **31 (4)**, 819-834.

Zhang, J. and E. W. Gill, 2006: Extraction of ocean waves spectra from simulated noisy bistatic high-frequency radar data, *IEEE Journal of Oceanic Engineering*, **31 (4)**, 779-796.